

# Bayesian inference for the stochastic identification of elastoplastic material parameters: Introduction, misconceptions and additional insight

H. Rappel<sup>a,b</sup>, L.A.A. Beex<sup>a,\*</sup>, J.S. Hale<sup>a</sup>, S.P.A. Bordas<sup>a,c,d</sup>

<sup>a</sup>*Faculty of Science, Technology and Communication, University of Luxembourg, Campus Kirchberg, 6, Rue Coudenhove-Kalergi, L-1359 Luxembourg, Luxembourg.*

<sup>b</sup>*Department of Aerospace and Mechanical Engineering, University of Liège, Chemin des Chevreuils 1, B-4000 Liège, Belgium.*

<sup>c</sup>*School of Engineering, Cardiff University, Queens Buildings, The Parade, Cardiff CF243AA, Wales, UK.*

<sup>d</sup>*Adjunct Professor, Intelligent Systems for Medicine Laboratory School of Mechanical and Chemical Engineering, The University of Western Australia, 35 Stirling Highway, Crawley/Perth WA 6009, Australia.*

---

## Abstract

Bayesian inference (BI) can be used for the probabilistic identification of material parameters. For inverse models for instance, BI may be considered convenient as it introduces a statistical regularisation. Understanding the concepts and the application of BI is however not trivial if one is only familiar with identification approaches based on error minimisation. This is particularly true when one is interested in elastoplastic material parameters. This contribution aims to shed light on the use of BI for the identification of elastoplastic material parameters. For this purpose a single spring is considered, for which the stress-strain curves are artificially created. Besides offering an introduction to BI, the main novelty of this contribution is the formulation to not only incorporate statistical errors in the measured stresses, but also statistical errors in the measured strains. Furthermore, a number of possible misconceptions on BI are highlighted based on the purely elastic case.

**Keywords:** Bayesian inference, Bayes' theorem, stochastic identification, statistical identification, parameter identification, elastoplasticity, plasticity

---

## 1. Introduction

Perhaps the most conventional way to identify material parameters in mechanics is to formulate an error function that measures the difference between the response of a model and the experimental data [1]. This error functional is then minimised with respect to the material parameters of interest to determine them. An alternative, and rather different approach is to use Bayesian inference (BI). Using Bayes' theorem a probability density function (PDF), the so-called posterior distribution (or simply posterior), can be formulated as a function of the material parameters of interest. Subsequently, the PDF is analysed to determine relevant values, such as the mean of the material parameters, the material properties at which the PDF is maximum and the covariance. Only for simplistic cases the PDF can be analysed analytically. Hence, most often numerical methods must be employed, e.g. Markov chain Monte Carlo (MCMC) techniques [2–5]. An alternative is to first approximate the PDF (e.g. by a Laplace approximation) and then analyse it [6, 7].

An advantage of BI, which conventional error minimisation approaches do not explicitly offer, is the possibility to incorporate the statistical noises of experimental devices [1]. Consequently, the identified material parameters come with a level of uncertainty. For inverse modelling based on BI, an advantage is that a regularisation is included which makes ill-posed problems still solvable [8]. On the other hand, applying Bayes' theorem for material parameter identification does require the measurement noise to be

---

\*Corresponding author

Email address: [lars.beex@uni.lu](mailto:lars.beex@uni.lu) (L.A.A. Beex)

known. In more detail, the noise distributions and the parameters of these distributions must be established. The numerical techniques to analyse the PDF may furthermore need careful attention.

The developments of BI in the field of parameter identification for mechanical models started with the identification of elastic constants. Isenberg [9] proposed a Bayesian approach for the identification of elastic parameters in 1979. This framework was subsequently used by various researchers to identify elastic material parameters based on dynamic responses [6, 10, 11]. Lai and Ip [12] used BI to identify the elastic properties of a thin composite plate. Daghia et al. [13] used the Bayesian framework for the dynamic identification of the elastic constants of thick laminated composite plates. Koutsourelakis [14] used Bayesian inference to identify spatially varying elastic material parameters. In 2010 Gogu et al. [1] presented an introduction in the Bayesian approach for the identification of elastic constants, and compared the results with those of error minimisation. The influence of prior knowledge has to date not been systematically studied. In another study, Gogu et al. [15] used the Bayesian framework to identify elastic constants in multi-directional laminates.

BI has also been used for parameter identification of nonlinear constitutive models. Muto and Beck [16] and Liu and Au [17] used the approach for hysteretic models, whereas Fitzenz et al. [18] used BI for a creep model of quartz. Most [19] used the Bayesian updating procedure for the parameter identification of an elastoplastic model without hardening (perfect plasticity). Rosic et al. [20] used linear Bayesian updating via polynomial chaos expansion for an elastoplastic system. Hernandez et al. [21] used BI for a viscoelastic material.

Another study that uses Bayes' theorem to identify material parameters is the work of Nichols et al. [22]. They employed the Bayesian approach to identify the nonlinear stiffness of a dynamic system. Furthermore, Nichols et al. [22] used the method to find the location, size and depth of delamination in a composite beam. Abhinav and Manohar [23] used BI to characterise the dynamic parameters of a structural system with geometrical nonlinearities. The approach is also employed as a framework to assess the quality of different models with respect to measured data (i.e. model selection): e.g. hyperelastic constitutive models for soft tissue [24], phenomenological models for tumour growth [25], models for damage progression in composites due to fatigue [26] and fatigue models for metals [27]. Sarkar et al. [28] used the Bayesian method to identify thermodynamical parameters of cementitious materials. BI is also used in the field of mechanics for inverse problems employing differential equations [3, 29].

Based on the high level of detail in the previous studies, it may not be clear for those who are not familiar with BI, how to apply it to the parameter identification of general elastoplastic models (e.g. with nonlinear hardening). It may also not be easy to understand how the prior knowledge, required to apply Bayes' theorem, influences the results. To the best of the authors' knowledge no studies in the field of mechanics have presented a way to incorporate uncertainties in the measured stresses, as well as uncertainties in the measured strains. In fields other than mechanics, studies can be found that deal with two error sources [30–35], but they focus on linear regression and not on nonlinear responses as required for nonlinear hardening.

This contribution therefore aims to introduce how Bayesian inference can be applied for the stochastic identification of elastoplastic material parameters. The important issues focused on are

- (1) a consistent formulation to incorporate the split in the purely elastic part of the response and the elastoplastic part,
- (2) a consistent formulation to incorporate the uncertainty in the measured stresses as well as the uncertainty in the measured strains for elastic(-plastic) models and
- (3) the presentation of possible misconceptions of BI.

The partial focus on possible misconceptions is quintessential, because they may not be trivial for those not familiar with BI. The elastic case is used as an illustration for this, because it is the simplest case to grasp.

The current contribution focuses on one dimensional stress-strain results of a single spring in order to be as straightforward as possible. A single spring is however not much more than an isotropic material model with no influence of the Poisson's ratio and hence, it is a useful first step to focus on. This contribution furthermore proposes a Bayesian framework to not only take the statistical errors in the stress into account,

but also the statistical error in the strain. The latter part shows similarities with the study of Kelly [34] in 2007, by computing the likelihood function considering all measured data, and the marginalisation integral.

The structure of the paper is as follows. Section 2 discusses the theoretical fundamentals behind Bayes' theorem, the elastoplastic material models and MCMC methods as the numerical techniques to analyse the posterior distribution. Section 3 describes a Bayesian approach for the stochastic identification of elastoplastic material parameters, when only the stress measurements include stochastic errors. Section 3 presents how to split the experimental data in a purely elastic domain and an elastoplastic domain. In section 4 the Bayesian method to incorporate both the statistical errors in the stresses and strains is presented. In section 5 a considerable number of relevant examples for all the aforementioned approaches is presented. Furthermore, in this section some misconceptions about the Bayesian method are indicated. In section 6 conclusions are finally presented.

## 2. Concepts

A conventional procedure to identify material parameters in mechanics relies on error minimisation. Often, a least-squared error function is formulated that measures the squared difference between the experimental data and the predicted model response. This error function is subsequently minimised with respect to the material parameters of interest. A measure for the quality of the model response with respect to the measured data is then formed by the residual (i.e. the final least-squared difference between the measured data and the model response).

Identification approaches based on BI aim to construct a probability distribution function (PDF) based on the measured data, as a function of the material parameters of interest. In the case of one parameter, the PDF measures the probability that a particular value of the parameter occurs. Hence, the PDF must be analysed to investigate which values the parameter will most probably be. Important quantities of interest are the PDF's maxima (i.e. 'modes' in general statistical terminology or 'maximum-a-posteriori-probability', abbreviated to 'MAP', in Bayesian terminology), the mean and the correlation.

BI may be considered as an approach that 'accounts' for the fact that only a limited number of observations are made. This is achieved by incorporating some assumed prior knowledge about the parameters of interest. For inverse modelling, the prior knowledge (prior distribution, or simply 'prior' in Bayesian terminology) regularises the inverse problem. This ensures that the systems to be solved are not ill-posed.

Note that conventional error minimisation approaches based on least-squares, are the same as the frequentist approach based on the maximum likelihood (ML), if the statistical error is additive, uncorrelated and normally distributed with a zero standard deviation [8]. Note that in the limit of an infinite number of measurements, the frequentist approach based on maximum likelihood and the Bayesian approach tend to the same results [36].

The remainder of this section presents the essential concepts of how to apply BI to the identification of elastoplastic material parameters in the case of a single spring. The concepts involve Bayes' theorem, the material models of interest and the adaptive MCMC method to analyse the posterior distributions.

### 2.1. Bayesian inference

We start by considering events  $A$  and  $B$ , and the discrete probabilities of each event:  $P(A)$  and  $P(B)$ . The probability that events  $A$  and  $B$  both occur, is given by the joint probability,  $P(A, B)$ , which can be expanded as:

$$P(A, B) = P(A|B)P(B) = P(B|A)P(A), \quad (1)$$

where  $P(A|B)$  and  $P(B|A)$  are conditional probabilities. The conditional probability  $P(A|B)$  expresses the probability that event  $A$  occurs, if it is certain that event  $B$  occurs. Using Eq. (1), the simplest form of Bayes' theorem can be written as:

$$P(A|B) = \frac{P(A)P(B|A)}{P(B)}. \quad (2)$$

If one regards two continuous random variables  $\mathbf{X} \in \mathbb{R}^n$  and  $\mathbf{Y} \in \mathbb{R}^k$  instead of discrete variables (bold capital letters in this subsection represent random variables), Eq. (2) can be rewritten in terms of the following probability distribution functions (where  $\pi$  denotes a PDF):

$$\pi(\mathbf{x}|\mathbf{y}) = \frac{\pi(\mathbf{x})\pi(\mathbf{y}|\mathbf{x})}{\pi(\mathbf{y})}, \quad (3)$$

where  $\pi(\mathbf{x})$ ,  $\pi(\mathbf{y}|\mathbf{x})$  and  $\pi(\mathbf{x}|\mathbf{y})$  are referred to as the prior distribution, the likelihood function and the posteriori distribution, respectively. In an identification problem,  $\mathbf{x}$  is the vector with  $n$  unknown parameters and  $\mathbf{y}$  is the vector with  $k$  observations.

Using the law of total probabilities [37] which relates the marginal probabilities ( $\pi(\mathbf{x})$  and  $\pi(\mathbf{y})$ ) to the conditional probabilities ( $\pi(\mathbf{y}|\mathbf{x})$ ), the denominator in Eq. (3) can be written as:

$$\pi(\mathbf{y}) = \int_{\mathbb{R}^n} \pi(\mathbf{x})\pi(\mathbf{y}|\mathbf{x})d\mathbf{x}. \quad (4)$$

Since the data ( $\mathbf{y}$ ) is already measured, the denominator in Eq. (3) is a constant number,  $C \in \mathbb{R}_{\geq 0}$ . This constant number can be regarded as a normalisation factor that ensures that integral of the posterior ( $\pi(\mathbf{x}|\mathbf{y})$ ) equals 1:

$$\pi(\mathbf{x}|\mathbf{y}) = \frac{1}{C} \pi(\mathbf{x})\pi(\mathbf{y}|\mathbf{x}). \quad (5)$$

In the case of parameter identification, one is not necessarily interested in the absolute values of the PDF but only in the relative values. In that case, the value of  $C$  is not important and hence, it suffices to rewrite Eq. (5) as:

$$\pi(\mathbf{x}|\mathbf{y}) \propto \pi(\mathbf{x})\pi(\mathbf{y}|\mathbf{x}). \quad (6)$$

In order to obtain the posterior (i.e. the PDF of the unknown parameters vector given the observations  $\pi(\mathbf{x}|\mathbf{y})$ ), the likelihood function ( $\pi(\mathbf{y}|\mathbf{x})$ ) and the prior ( $\pi(\mathbf{x})$ ) need to be formulated. First, the likelihood function is considered.

In order to construct the likelihood function, a noise model has to be formulated and a noise distribution ( $\pi_{\text{noise}}$ ) has to be determined and calibrated. For the moment, we assume that the noise distribution is known (including its parameters). The noise model used in this study is additive, which is frequently employed, amongst others in several inverse studies [8, 13]. The additive noise model can be written as follows:

$$\mathbf{Y} = f(\mathbf{X}) + \mathbf{\Omega}, \quad (7)$$

where  $\mathbf{X} \in \mathbb{R}^n$  is the vector of unknown material parameters,  $\mathbf{Y} \in \mathbb{R}^k$  the vector of the measured data and  $\mathbf{\Omega} \in \mathbb{R}^k$  the noise vector.  $f : \mathbb{R}^n \rightarrow \mathbb{R}^k$  represents the model and is a function of the unknown material parameters ( $\mathbf{X}$ ). Given the realisations  $\mathbf{X} = \mathbf{x}$  and  $\mathbf{\Omega} = \boldsymbol{\omega}$ , and assuming that the input ( $\mathbf{X}$ ) and the error ( $\mathbf{\Omega}$ ) are statistically independent, the likelihood function reads:

$$\pi(\mathbf{y}|\mathbf{x}) = \pi_{\text{noise}}(\mathbf{y} - f(\mathbf{x})), \quad (8)$$

where  $\pi_{\text{noise}}(\boldsymbol{\omega})$  is the PDF of the noise (which is assumed to be identified based on separate calibration experiments). Substitution of Eq. (8) in Eq. (6) yields:

$$\pi(\mathbf{x}|\mathbf{y}) \propto \pi(\mathbf{x})\pi_{\text{noise}}(\mathbf{y} - f(\mathbf{x})). \quad (9)$$

Perhaps the most critical aspect of the Bayesian framework is the selection of the prior distribution ( $\pi(\mathbf{x})$ ) [8] in which pre-existing knowledge about the parameters is translated in terms of a PDF. Note however if enough data is observed the prior hardly has any influence [24]. The influence of the prior distribution will be considered in more detail in section 5.

Once the posterior is formulated (Eq. (9)), it is used to compute the unknown parameters and the corresponding statistical properties in an analytical or numerical manner (e.g. using Markov chain Monte



Carlo methods). The adaptive Markov chain Monte Carlo is considered in subsection 2.3, as it is the numerical approach employed in this contribution to evaluate the posteriors.

## 2.2. Material models

In this contribution, BI is developed to identify the parameters of four one-dimensional material models: linear elasticity, linear elasticity with perfect plasticity, linear elasticity with linear hardening and linear elasticity with nonlinear hardening. Hardening is considered to be kinematic and associative. For each model, the identification is based on the results of monotonic uniaxial tensile tests. Below, the governing equations of the models are given, as well as those for when monotonic tensile loading takes place.

### 2.2.1. Linear elastic

The linear elastic model expresses a material behaviour by assuming a linear relationship between the stresses and strains:

$$\sigma(\epsilon, \mathbf{x}) = E\epsilon, \quad (10)$$

where  $\sigma$  is the stress,  $\epsilon$  is the strain,  $\mathbf{x}$  is the material parameter vector (here  $\mathbf{x} = E$ ) and  $E$  is Young's modulus. This expression remains unchanged for the case of monotonic tensile loading.

### 2.2.2. Linear elastic-perfectly plastic

The linear elastic-perfectly plastic model neglects the effect of work hardening, assuming that purely plastic deformation occurs when the stress reaches its yield value. The total strain ( $\epsilon$ ) in this contribution is additively split into an elastic part  $\epsilon_e$  and a plastic part  $\epsilon_p$ :

$$\epsilon = \epsilon_e + \epsilon_p, \quad (11)$$

and the stress is defined as a function of the elastic strain,  $\epsilon_e$ :

$$\sigma(\epsilon, \mathbf{x}) = E\epsilon_e = E(\epsilon - \epsilon_p). \quad (12)$$

The yield condition at which plastic yielding occurs, is written as:

$$f(\sigma) = |\sigma| - \sigma_{y0} \leq 0, \quad (13)$$

where  $\sigma_{y0}$  is the initial yield stress and  $f$  is the yield function. Consequently,  $\mathbf{x} = [E \quad \sigma_{y0}]^T$ .

Furthermore, the flow rule for the plastic strain can be written as:

$$\dot{\epsilon}_p = \dot{\alpha} \frac{\partial f}{\partial \sigma} = \dot{\alpha} \text{sgn}(\sigma), \quad (14)$$

where  $\text{sgn}(\cdot)$  is the sign function and  $\alpha$  is the cumulative plastic strain. Finally, the Kuhn-Tucker conditions [38] must hold:

$$\dot{\alpha} \geq 0, \quad f(\sigma) \leq 0, \quad \dot{\alpha} f(\sigma) = 0. \quad (15)$$

The stress-strain response of the linear elastic-perfectly plastic model during monotonic tension can be written as:

$$\sigma = \begin{cases} E\epsilon & \text{if } \epsilon \leq \frac{\sigma_{y0}}{E} \\ \sigma_{y0} & \text{if } \epsilon > \frac{\sigma_{y0}}{E} \end{cases}. \quad (16)$$

Using the Heaviside step function ( $h(\cdot)$ ), Eq. (16) can be expressed as:

$$\sigma(\epsilon, \mathbf{x}) = E\epsilon \left( 1 - h\left(\epsilon - \frac{\sigma_{y0}}{E}\right) \right) + \sigma_{y0} h\left(\epsilon - \frac{\sigma_{y0}}{E}\right). \quad (17)$$

### 2.2.3. Linear elastic-linear hardening

The linear elastic-linear hardening model is identical to the linear elastic-perfectly plastic model, except for the yield function, which writes:

$$f(\sigma) = |\sigma| - \sigma_{y0} - H\alpha \leq 0, \quad (18)$$

where  $H$  is the plastic modulus. Here,  $\mathbf{x} = [E \quad \sigma_{y0} \quad H]^T$ .

Consequently, the stress-strain response of the model during monotonic tension writes:

$$\sigma = \begin{cases} E\epsilon & \text{if } \epsilon \leq \frac{\sigma_{y0}}{E} \\ \sigma_{y0} + H\epsilon_p & \text{if } \epsilon > \frac{\sigma_{y0}}{E} \end{cases}, \quad (19)$$

which can again be expressed using the Heaviside step function:

$$\sigma(\epsilon, \mathbf{x}) = E\epsilon \left( 1 - h\left(\epsilon - \frac{\sigma_{y0}}{E}\right) \right) + \left( \sigma_{y0} + \frac{HE}{H+E} \left( \epsilon - \frac{\sigma_{y0}}{E} \right) \right) h\left(\epsilon - \frac{\sigma_{y0}}{E}\right). \quad (20)$$

### 2.2.4. Linear elastic-nonlinear hardening

The linear elastic-nonlinear hardening model only differs from the linear elastic-perfectly plastic model through the yield function which writes:

$$f(\sigma) = |\sigma| - \sigma_{y0} - H\alpha^n \leq 0, \quad (21)$$

where  $n$  is an additional plastic material parameter and hence,  $\mathbf{x} = [E \quad \sigma_{y0} \quad H \quad n]^T$ .

For the monotonic loading case, the stress-strain response can be written as:

$$\sigma = \begin{cases} E\epsilon & \text{if } \epsilon \leq \frac{\sigma_{y0}}{E} \\ \sigma_{y0} + H\epsilon_p^n & \text{if } \epsilon > \frac{\sigma_{y0}}{E} \end{cases}, \quad (22)$$

or using the Heaviside step function:

$$\sigma(\epsilon, \mathbf{x}) = E\epsilon \left( 1 - h\left(\epsilon - \frac{\sigma_{y0}}{E}\right) \right) + \left( \sigma_{y0} + H \left( \epsilon - \frac{\sigma_{y0}}{E} \right)^n \right) h\left(\epsilon - \frac{\sigma_{y0}}{E}\right). \quad (23)$$

It is important to note that Eq. (23) is an implicit function of the stress ( $\sigma(\epsilon, \mathbf{x})$  appears both on the left hand side and right hand side of Eq. (23) and cannot immediately be identified from Eq. (23)). This is in contrast to the stress-strain expressions of the previous material models for monotonic tension (Eqs. (10), (17) and (20)), which are all explicit functions (i.e.  $\sigma(\epsilon, \mathbf{x})$  can be directly computed when one has  $\epsilon$ ). This changes the likelihood function construction procedure for the linear elastic-nonlinear hardening case which is discussed in subsection 3.4.

### 2.3. Markov chain Monte Carlo method (MCMC)

Once a posterior has been constructed, it needs to be analysed to determine the unknown parameters. Only in a few straightforward cases, the analysis can be performed analytically. A numerical approach needs to be employed in the majority of the cases, e.g. when the model is nonlinear or when the model is an implicit function. If the posterior is continuous one may use approximation approaches (e.g. a Laplace approximation [6]) that require the derivatives of the posterior. If the posterior is  $C_0$ -continuous however, numerical approaches which do not require any derivatives need to be employed. The posteriors for the aforementioned elastoplastic models are all  $C_0$ -continuous due to the abrupt transition between the purely elastic part and the elastoplastic part of the response (see e.g. Eq. (22)).

Markov chain Monte Carlo (MCMC) techniques are frequently employed numerical approaches to investigate posteriors, that do not require any derivatives [39–41]. MCMC approaches are based on drawing samples from the posterior to approximate the parameters' statistical properties (e.g. the mean value and variance). Below, the fundamental concepts of the Monte Carlo method are discussed as well as the adaptive Metropolis algorithm to perform the sampling.

### 2.3.1. Monte Carlo method

The main purpose of the Monte Carlo method is to approximate integrals of the following form:

$$I = \int_{\mathbb{R}^n} g(\mathbf{x})\pi(\mathbf{x})d\mathbf{x}, \quad (24)$$

where  $\pi$  is the PDF of interest (in our case the posterior) and  $g$  is an integrable function over  $\mathbb{R}^n$ . This integral can be approximated using the following quadrature:

$$\hat{I} = \frac{1}{N} \sum_{i=1}^N g(\mathbf{x}_i), \quad (25)$$

where  $\{\mathbf{x}_i\}_i^N$  is the set of samples drawn from the PDF of interest,  $\pi$ , and the hat on  $\hat{I}$  represents the numerically approximated counterpart of  $I$ . The drawing of samples from  $\pi$  implies that most of the samples are in the domain where  $\pi \neq 0$ . By the law of large numbers (LLN) [42],  $\hat{I}$  converges as follows:

$$\lim_{N \rightarrow +\infty} \frac{1}{N} \sum_{i=1}^N g(\mathbf{x}_i) = I. \quad (26)$$

Similarly, the variance of  $g(\mathbf{x})$  can be estimated by [43]:

$$\widehat{\text{var}}(g(\mathbf{x})) = \frac{1}{N} \sum_{i=1}^N \left( g(\mathbf{x}_i) - \hat{I}_N \right)^2, \quad (27)$$

where  $\widehat{\text{var}}$  is the numerically approximated variance.

The posterior mean of  $\mathbf{x}$  ( $\boldsymbol{\mu}_{\text{post}}$ ) can be computed by substituting  $g(\mathbf{x}) = \mathbf{x}$  in Eq. (25), which yields:

$$\boldsymbol{\mu}_{\text{post}} = \int_{\mathbb{R}^n} \mathbf{x} \pi(\mathbf{x}) d\mathbf{x} = \lim_{N \rightarrow +\infty} \frac{1}{N} \sum_{i=1}^N \mathbf{x}_i. \quad (28)$$

The approximated variance reads in that case:

$$\widehat{\text{var}}(\mathbf{x}) = \frac{1}{N} \sum_{i=1}^N \left( \mathbf{x}_i - \mathbf{x}_{\text{mean}} \right)^2. \quad (29)$$

If we again assume that a large number of samples is taken (i.e.  $N$  is large), the MAP estimate can furthermore be approximated as [42]:

$$\mathbf{MAP} = \underset{\mathbf{x}_i, i=1, \dots, N}{\text{argmax}} \pi(\mathbf{x}_i). \quad (30)$$

The essential part of a Monte Carlo procedure is the drawing of admissible samples ( $\mathbf{x}_i$ ). Below, the standard and adaptive Metropolis algorithms are discussed. The adaptive one is the algorithm used in section 5.

### 2.3.2. The standard and the adaptive Metropolis algorithm

The standard Metropolis-Hastings approach is a frequently employed MCMC algorithm [42]. The basic idea of the Metropolis-Hastings algorithm is to explore the PDF of interest by making a random walk across the parameter space  $\mathbf{x}$ . Considering sample  $\mathbf{x}_i$  and an evaluation of the PDF  $\pi(\mathbf{x}_i)$ , a new sample  $\mathbf{x}_p$  is proposed by drawing from a proposal distribution ( $q$  in Algorithm 1). If the PDF evaluated at the proposed sample ( $\pi(\mathbf{x}_p)$ ) is larger than at the current sample ( $\pi(\mathbf{x}_i)$ ), the proposed sample is *always* accepted. However, if the PDF at the proposed sample is smaller than at the current sample, the proposed sample *may* be accepted based on the ratio of the PDF evaluated at the proposed and current sample ( $r$  in Algorithm 1). The ratio is compared to a random number generated from a uniform distribution. If the ratio is greater

than the random number, the proposed sample is accepted. If the ratio is smaller than the random number, the proposed sample is rejected, and we remain at the current sample. In the case the proposed sample was accepted, the proposed sample becomes the current sample. The algorithm repeats until convergence is achieved.

Critically, as the number of samples increases, it can be shown that the distribution of values approximates the target distribution. For more information, see [43]. The standard Metropolis-Hastings algorithm is presented in Algorithm 1 in more detail.

---

**Algorithm 1** The standard Metropolis-Hastings algorithm

---

```

1: select the initial sample  $\mathbf{x}_0 \in \mathbb{R}^n$  and  $\gamma$ 
2: for  $i = 0, 1, 2, \dots, N - 1$  do
3:   draw  $\mathbf{x}_p \in \mathbb{R}^n$  from the proposal distribution  $q(\mathbf{x}_p|\mathbf{x}_i)$  in Eq. (33)
4:   calculate the ratio  $r(\mathbf{x}_i, \mathbf{x}_p) = \min\left(1, \frac{\pi(\mathbf{x}_p)q(\mathbf{x}_i|\mathbf{x}_p)}{\pi(\mathbf{x}_i)q(\mathbf{x}_p|\mathbf{x}_i)}\right)$   $\triangleright \pi(\cdot)$  denotes the target distribution
      (i.e. posterior).
5:   draw  $u \in [0, 1]$  from uniform probability density
6:   if  $r(\mathbf{x}_i, \mathbf{x}_p) \geq u$  then
7:      $\mathbf{x}_{i+1} = \mathbf{x}_p$ 
8:   else
9:      $\mathbf{x}_{i+1} = \mathbf{x}_i$ 
10:  end if
11: end for

```

---

In the case that the transition kernel is symmetric (as in this contribution), the following relation holds:

$$q(\mathbf{x}_i|\mathbf{x}_p) = q(\mathbf{x}_p|\mathbf{x}_i). \quad (31)$$

Consequently, step 4 in the algorithm simplifies to:

$$r(\mathbf{x}_i, \mathbf{x}_p) = \min\left(1, \frac{\pi(\mathbf{x}_p)}{\pi(\mathbf{x}_i)}\right). \quad (32)$$

The stability and convergence of the algorithm can be checked by tracing the generated samples and analysing their characteristics. The evolution of the mean value and the standard deviation can for instance be checked for convergence [28]. The distribution approximated by MCMC converges to the target distribution if the samples show a stationary statistical behaviour, i.e. if the mean and standard deviation remain constant [28].

The efficiency of the algorithm is influenced by the initial sample ( $\mathbf{x}_0$ ) and the proposal distribution ( $q$ ) [8]. The most common proposal distribution for the Metropolis-Hastings algorithm (as employed here) is of the following Gaussian form:

$$q(\mathbf{x}_i|\mathbf{x}_p) = q(\mathbf{x}_p|\mathbf{x}_i) \propto \exp\left(-\frac{1}{2\gamma^2} \|\mathbf{x}_i - \mathbf{x}_p\|^2\right), \quad (33)$$

where  $\gamma$  is the parameter that determines the width of the proposal distribution and must be tuned to obtain an efficient and converging algorithm. An efficient starting value is  $\gamma = \frac{2.38}{\sqrt{n}}$  [44], where  $n$  is the number of unknown parameters and hence, the dimension of the posterior.

To overcome the tuning of  $\gamma$ , Haario et al. [45] introduced the Adaptive Proposal (AP). The AP method updates the width of the proposal distribution, based on the existing knowledge of the posterior. The existing knowledge is based on the previous samples. For sample  $i + 1$ , the update employs the following formulation:

$$q(\mathbf{x}_p|\mathbf{x}_i) \sim N(\mathbf{x}_i, \gamma^2 \mathbf{R}_i), \quad (34)$$

where  $N(\mathbf{x}_i, \gamma^2 \mathbf{R}_i)$  denotes a normal distribution with mean  $\mathbf{x}_i$  and covariance matrix  $\gamma^2 \mathbf{R}_i$ , of size  $n \times n$ . To establish  $\mathbf{R}_i$ , all  $i$  previous samples are first stored in matrix  $\mathbf{K}$  of size  $i \times n$ .  $\mathbf{R}_i$ , is then computed as:

$$\mathbf{R}_i = \frac{1}{i-1} \tilde{\mathbf{K}}^T \tilde{\mathbf{K}}, \quad (35)$$

where  $\tilde{\mathbf{K}} = \mathbf{K} - \mathbf{K}_{\text{mean}}$  and  $\mathbf{K}_{\text{mean}}$  reads:

$$\mathbf{K}_{\text{mean}} = \begin{bmatrix} \mathbf{k}_{\text{mean}} \\ \mathbf{k}_{\text{mean}} \\ \vdots \\ \mathbf{k}_{\text{mean}} \end{bmatrix}_{i \times n}, \quad (36)$$

and  $\mathbf{k}_{\text{mean}}$  is a row matrix of length  $n$  which is determined as follows:

$$\mathbf{k}_{\text{mean}} = \frac{1}{i} \begin{bmatrix} \sum_{j=1}^i (K)_{j1} & \sum_{j=1}^i (K)_{j2} & \cdots & \sum_{j=1}^i (K)_{jn} \end{bmatrix}. \quad (37)$$

The following relation is used for  $N(\mathbf{x}_i, \gamma^2 \mathbf{R}_i)$  in this contribution:

$$N(\mathbf{x}_i, \gamma^2 \mathbf{R}_i) = \mathbf{x}_i + \frac{\gamma}{\sqrt{i-1}} \tilde{\mathbf{K}}^T N(0, \mathbf{I}_i), \quad (38)$$

where  $\mathbf{I}_i$  is the identity matrix of size  $i \times i$  and  $N(0, \mathbf{I}_i)$  is the  $i$ -dimensional normal distribution.

Note that it is computationally inefficient to update the proposal distribution after each new sample is generated. In the numerical examples in this study therefore, updating takes place once per 1000 sample generations. Algorithm 2 shows the Metropolis-Hastings algorithm with the symmetric AP proposal (Eq. (38)) that is employed here.

---

**Algorithm 2** The Metropolis-Hastings algorithm with symmetric AP proposal

---

```

1: select the initial sample  $\mathbf{x}_0 \in \mathbb{R}^n$  and set  $\gamma = \frac{2.38}{\sqrt{n}}$ 
2: for  $i = 0, 1, 2, \dots, N-1$  do
3:   draw  $\mathbf{x}_p \in \mathbb{R}^n$  from the proposal distribution  $q(\mathbf{x}_p|\mathbf{x}_i)$  in Eq. (38)
4:   calculate the ratio  $r(\mathbf{x}_i, \mathbf{x}_p) = \min\left(1, \frac{\pi(\mathbf{x}_p)}{\pi(\mathbf{x}_i)}\right)$   $\triangleright \pi(\cdot)$  denotes the target distribution (i.e. posterior).
5:   draw  $u \in [0, 1]$  from uniform probability density
6:   if  $r(\mathbf{x}_i, \mathbf{x}_p) \geq u$  then
7:      $\mathbf{x}_{i+1} = \mathbf{x}_p$ 
8:   else
9:      $\mathbf{x}_{i+1} = \mathbf{x}_i$ 
10:  end if
11:  per 1000 samples
12:    update matrix  $\tilde{\mathbf{K}}$ 
13: end for
```

---

### 3. Bayesian inference for tensile tests with noise in the stress

The current section focuses on the formulation of Bayesian identification approaches for the material models of subsection 2.2, when only the stress measurements are polluted with statistical errors. The measured strains are thus considered to be exact. In section 4, Bayesian updating is considered when also the measured strains are also polluted with a statistical noise.

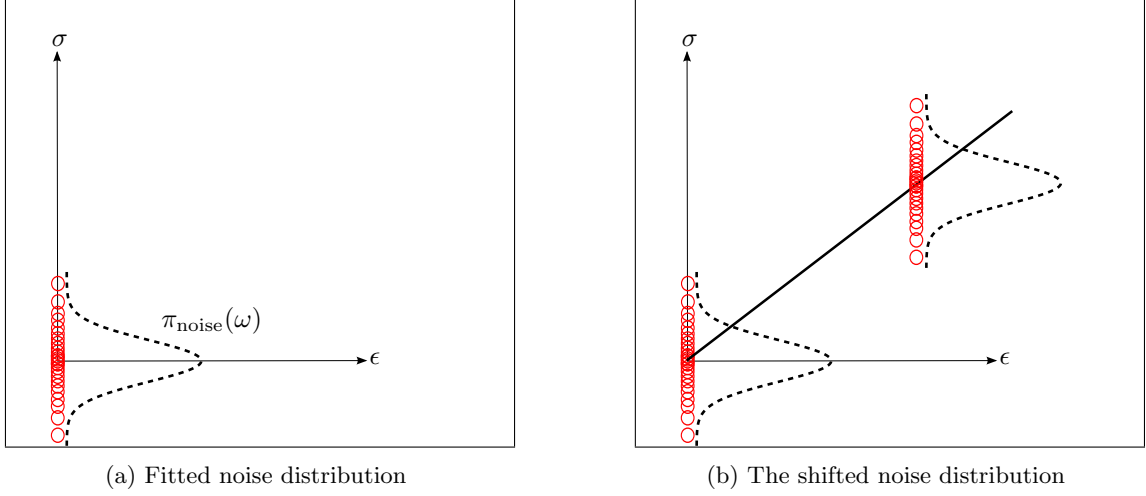


Figure 1: Schematic of the stress-strain measurements (red circles) of the ‘calibration experiments’, including the noise distributions (dashed). The theoretical stress-strain relation (which is exact for the calibration experiments) is presented as the bold straight line on the diagram on the right.

### 3.1. Noise distribution

To determine the noise distribution and its parameters, two sets of ‘calibration experiments’ can be performed. First, a test is performed without any specimen. The stress-strain measurements of this test are shown in Fig. 1(a). It shows that the PDF of the noise in the ‘stress measurements’ is a normal distribution with a zero mean and a standard deviation of  $S_{\text{noise}}$ .

Second, the evolution of the noise distribution (including its parameters) must be determined. To this purpose, a tensile test is performed on a calibration specimen (of which the Young’s modulus is known). The assumed results are presented in Fig. 1(b). The mean stress value varies linearly with the strain. The standard deviation  $S_{\text{noise}}$  however remains the same.

As the ‘calibration measurements’ indicate that an additive noise model can be used and the stresses are polluted by a normal noise distribution with standard deviation  $S_{\text{noise}}$ , BI is first employed to identify the Young’s modulus of the linear elastic model.

### 3.2. Linear elastic

The only unknown material parameter in the linear elastic model is the Young’s modulus ( $E$ ). Based on section 2, the additive noise model for a single stress measurement can be written as follows:

$$\sigma^m = E\epsilon + \Omega, \quad (39)$$

where  $\sigma^m$  is the measured stress and  $\Omega$  is the random variable representing the noise in the stress measurement. Based on the artificially generated calibration results, the noise distribution is normal and can be written as:

$$\pi_{\text{noise}}(\omega) = \frac{1}{\sqrt{2\pi}S_{\text{noise}}} \exp\left(-\frac{\omega^2}{2S_{\text{noise}}^2}\right). \quad (40)$$

Using Eq. (8), the likelihood function is expanded as:

$$\pi(\sigma^m|E) = \pi_{\text{noise}}(\sigma^m - E\epsilon) = \frac{1}{\sqrt{2\pi}S_{\text{noise}}} \exp\left(-\frac{(\sigma^m - E\epsilon)^2}{2S_{\text{noise}}^2}\right), \quad (41)$$

Substitution of Eq. (41) in Eq. (9) then yields the following expression for the posterior:

$$\pi(E|\sigma^m) \propto \pi(E) \exp\left(-\frac{(\sigma^m - E\epsilon)^2}{2S_{\text{noise}}^2}\right). \quad (42)$$

If we use a prior in the form of a modified normal distribution as follows:

$$\pi(E) \propto \begin{cases} \exp\left(-\frac{(E-\bar{E})^2}{2S_E^2}\right) & \text{if } E \geq 0 \\ 0 & \text{otherwise} \end{cases}, \quad (43)$$

the posterior distribution reads:

$$\pi(E|\sigma^m) \propto \begin{cases} \exp\left(-\left[\frac{(E-\bar{E})^2}{2S_E^2} + \frac{(\sigma^m - E\epsilon)^2}{2S_{\text{noise}}^2}\right]\right) & \text{if } E \geq 0 \\ 0 & \text{otherwise} \end{cases}, \quad (44)$$

where  $\bar{E}$  and  $S_E$  are the mean and standard deviation of the prior distribution, respectively. Note that the Young's modulus cannot be negative for an actual material, which is taken into account in the prior distribution (Eq. (43)).

If we now consider the posterior distribution of the previous measurement to be the prior distribution of the current measurement, the posterior for all  $k$  measurements can be expressed as:

$$\pi(E|\sigma^m) \propto \exp\left(-\left[\frac{(E-\bar{E})^2}{2S_E^2} + \frac{\sum_{i=1}^k (\sigma_i^m - E\epsilon_i)^2}{2S_{\text{noise}}^2}\right]\right), \quad E \geq 0 \quad (45)$$

where  $\pi(E|\sigma^m) = \pi(E|\sigma_1^m, \sigma_2^m, \dots, \sigma_k^m)$ . Eq. (45) can now be written in the following form:

$$\pi(E|\sigma^m) \propto \exp\left(-\frac{(E-\mu_{\text{post}})^2}{2S_{\text{post}}^2}\right), \quad E \geq 0 \quad (46)$$

where  $\mu_{\text{post}}$  and  $S_{\text{post}}$  are the mean and standard deviation of the posterior distribution, which is again a normal distribution (with the condition  $E \geq 0$ ). Both can be expressed as:

$$\mu_{\text{post}} = \frac{S_{\text{noise}}^2 \bar{E} + S_E^2 \sum_{i=1}^k \epsilon_i \sigma_i^m}{S_{\text{noise}}^2 + S_E^2 \sum_{i=1}^k \epsilon_i^2}, \quad S_{\text{post}} = \sqrt{\frac{S_{\text{noise}}^2 S_E^2}{S_{\text{noise}}^2 + S_E^2 \sum_{i=1}^k \epsilon_i^2}}. \quad (47)$$

Hence, it is possible to analytically examine the posterior distribution for the linear elastic model, in case the noise model is additive and the noise distribution as well as the prior distribution are (modified) normal distributions. For the other cases below, MCMC approaches are required and the adaptive MCMC approach used for those is verified based on the analytical expressions in Eq. (47) for the linear elastic model.

### 3.3. Linear elastic-perfectly plastic

The parameters to be identified for the linear elastic-perfectly plastic model are the Young's modulus and the initial yield stress which are stored in parameter vector  $\mathbf{x} = [E \quad \sigma_{y0}]^T$ . Since the experimental equipment and experimental condition both remain the same (i.e. the measured stresses are still polluted by noise stemming from the same normal distribution and the measured strains are still exact), the same additive noise model applies:

$$\sigma^m = \sigma(\epsilon, \mathbf{x}) + \Omega, \quad (48)$$

where  $\sigma(\epsilon, \mathbf{x})$  is referred to as the theoretical stress and takes the form of the stress-strain relation for monotonic tension in Eq. (16). Using Eq. (40) for the noise distribution, the likelihood function for a single stress measurement reads:

$$\pi(\sigma^m|\mathbf{x}) = \pi_{\text{noise}}(\sigma^m - \sigma(\epsilon, \mathbf{x})) = \frac{1}{\sqrt{2\pi}S_{\text{noise}}} \exp\left(-\frac{(\sigma^m - \sigma(\epsilon, \mathbf{x}))^2}{2S_{\text{noise}}^2}\right), \quad (49)$$

or:

$$\pi(\sigma^m|\mathbf{x}) = \frac{1}{\sqrt{2\pi}S_{\text{noise}}} \exp\left(-\frac{\left(\sigma^m - E\epsilon\left(1 - h\left(\epsilon - \frac{\sigma_{y0}}{E}\right)\right) - \sigma_{y0}h\left(\epsilon - \frac{\sigma_{y0}}{E}\right)\right)^2}{2S_{\text{noise}}^2}\right). \quad (50)$$

Taking the physical constraints into account that the Young's modulus and the initial yield stress must be nonnegative, the following prior distribution is selected:

$$\pi(\mathbf{x}) \propto \begin{cases} \exp\left(-\frac{(\mathbf{x}-\bar{\mathbf{x}})^T \mathbf{\Gamma}_{\mathbf{x}}^{-1}(\mathbf{x}-\bar{\mathbf{x}})}{2}\right) & \text{if } E \geq 0 \text{ and } \sigma_{y0} \geq 0 \\ 0 & \text{otherwise} \end{cases}, \quad (51)$$

where  $\bar{\mathbf{x}}$  is the mean value vector of the prior distribution and  $\mathbf{\Gamma}_{\mathbf{x}}$  is the covariance matrix of the prior. Substitution of Eq. (50) and Eq. (51) in the reduced variant of Bayes' formula of Eq. (9), yields the following posterior distribution for  $k$  measurements:

$$\pi(\mathbf{x}|\sigma^m) \propto \exp\left(-\left[\frac{(\mathbf{x}-\bar{\mathbf{x}})^T \mathbf{\Gamma}_{\mathbf{x}}^{-1}(\mathbf{x}-\bar{\mathbf{x}})}{2} + \frac{\sum_{i=1}^k \left(\sigma_i^m - E\epsilon_i\left(1 - h\left(\epsilon_i - \frac{\sigma_{y0}}{E}\right)\right) - \sigma_{y0}h\left(\epsilon_i - \frac{\sigma_{y0}}{E}\right)\right)^2}{2S_{\text{noise}}^2}\right]\right), \quad (52)$$

where the probability of obtaining a negative Young's modulus and initial yield stress is zero thanks to the selected prior distribution.

It is important to realise that the posterior distribution in this case is not of a form that allows an analytical evaluation due to the presence of the Heaviside function. Hence, the adaptive MCMC approach is employed to analyse the posterior for the linear elastic-perfectly plastic model in section 5.

### 3.4. Linear elastic-linear hardening

The parameter vector for the linear elastic-linear hardening model reads  $\mathbf{x} = [E \quad \sigma_{y0} \quad H]^T$ . Assuming the same experimental equipment and condition (and hence, the same noise model and noise distribution), the likelihood function for a single measurement reads:

$$\pi(\sigma^m|\mathbf{x}) \propto \exp\left(-\frac{\left(\sigma^m - E\epsilon\left(1 - h\left(\epsilon - \frac{\sigma_{y0}}{E}\right)\right) - \left(\sigma_{y0} + \frac{HE}{H+E}\left(\epsilon - \frac{\sigma_{y0}}{E}\right)\right)h\left(\epsilon - \frac{\sigma_{y0}}{E}\right)\right)^2}{2S_{\text{noise}}^2}\right). \quad (53)$$

In addition to the physical constraints for the Young's modulus and the initial yield stress, the plastic modulus ( $H$ ) must also be nonnegative. The following prior distribution is therefore selected:

$$\pi(\mathbf{x}) \propto \begin{cases} \exp\left(-\frac{(\mathbf{x}-\bar{\mathbf{x}})^T \mathbf{\Gamma}_{\mathbf{x}}^{-1}(\mathbf{x}-\bar{\mathbf{x}})}{2}\right) & \text{if } E \geq 0 \text{ and } \sigma_{y0} \geq 0 \text{ and } H \geq 0 \\ 0 & \text{otherwise} \end{cases}. \quad (54)$$

Using Bayes' formula, the posterior distribution for  $k$  observations reads:

$$\pi(\mathbf{x}|\sigma^m) \propto \exp\left(-\left[\frac{(\mathbf{x}-\bar{\mathbf{x}})^T \mathbf{\Gamma}_{\mathbf{x}}^{-1}(\mathbf{x}-\bar{\mathbf{x}})}{2} + \frac{\sum_{i=1}^k \left(\sigma_i^m - E\epsilon_i\left(1 - h\left(\epsilon_i - \frac{\sigma_{y0}}{E}\right)\right) - \left(\sigma_{y0} + \frac{HE}{H+E}\left(\epsilon_i - \frac{\sigma_{y0}}{E}\right)\right)h\left(\epsilon_i - \frac{\sigma_{y0}}{E}\right)\right)^2}{2S_{\text{noise}}^2}\right]\right). \quad (55)$$



### 3.5. Linear elastic-nonlinear hardening

The parameter vector for the linear elastic-nonlinear hardening model is  $\mathbf{x} = [E \ \sigma_{y0} \ H \ n]^T$ . Considering no change of experimental equipment (and hence, the same noise model and noise distribution), the expression for the measured stress reads again:

$$\sigma^m = \sigma(\epsilon, \mathbf{x}) + \Omega, \quad (56)$$

which, together with Eq. (23), results in the following expression for the measured stress:

$$\sigma^m = E\epsilon \left(1 - h\left(\epsilon - \frac{\sigma_{y0}}{E}\right)\right) + \left(\sigma_{y0} + H\left(\epsilon - \frac{\sigma_{y0}}{E}\right)^n\right)h\left(\epsilon - \frac{\sigma_{y0}}{E}\right) + \Omega. \quad (57)$$

It is important to note that the expression for the measured stress is now a function of the theoretical stress ( $\sigma(\epsilon, \mathbf{x})$ ). This is in contrast to the expressions of the measured stresses of the other material models. Consequently, the construction of the likelihood function changes. First, one needs to determine the probability that the measured stress occurs, for a given theoretical stress and a set of given material parameters:

$$\pi(\sigma^m | \mathbf{x}, \sigma(\epsilon, \mathbf{x})) = \pi_{\text{noise}}(\sigma^m - \sigma(\epsilon, \mathbf{x})). \quad (58)$$

The likelihood function required for Bayes' theorem however, expresses the likelihood that measured stresses occur for given parameters. This can be obtained by integrating Eq. (58), together with the theoretical stress likelihood function, over the theoretical stress [46]:

$$\pi(\sigma^m | \mathbf{x}) = \int_0^{+\infty} \pi(\sigma^m | \mathbf{x}, \sigma(\epsilon, \mathbf{x})) \pi(\sigma(\epsilon, \mathbf{x}) | \mathbf{x}) d\sigma. \quad (59)$$

In Eq. (59), the theoretical stress is integrated from 0 to infinity, because it cannot be smaller than zero in monotonic tension (otherwise compression would occur). As the theoretical stress can in principle be infinitely large, no true upper bound is included.

In the case that the parameters are given (as in MCMC approaches in which each sample is a realisation of the parameters), the theoretical stress likelihood function can be expressed as follows:

$$\pi(\sigma(\epsilon, \mathbf{x}) | \mathbf{x}) = \delta(\sigma(\epsilon, \mathbf{x}) - w), \quad (60)$$

where  $\delta$  is the Dirac delta function and  $w$  is used here to represent the right hand side of Eq. (23). Note that in the case that all the parameters are given, the only possible value for the theoretical stress is the same expression of the theoretical stress, but only as a function of the parameters. In Eq. (60) this is imposed by the Dirac delta function. Substitution of Eq. (58) and Eq. (60) in Eq. (59) yields:

$$\pi(\sigma^m | \mathbf{x}) = \int_0^{+\infty} \pi_{\text{noise}}(\sigma^m - \sigma(\epsilon, \mathbf{x})) \delta(\sigma(\epsilon, \mathbf{x}) - w) d\sigma. \quad (61)$$

The integral in Eq. (61) can be computed using [47]:

$$\int_a^b f(z) \delta(g(z)) dz = \begin{cases} \sum_{i=1}^n \frac{f(c_i)}{|g'(c_i)|} & \text{if } a < c_i < b \\ 0 & \text{otherwise} \end{cases}, \quad (62)$$

where  $c_i$  are the  $i$  roots of  $g(z)$ , for which holds  $\frac{dg(c_i)}{dz} \neq 0$ . Combining Eqs. (61) and (62) yields the final likelihood function for a single measurement as:

$$\pi(\sigma^m | \mathbf{x}) \propto \begin{cases} \exp\left(-\frac{(\sigma^m - E\epsilon)^2}{2S_{\text{noise}}^2}\right) & \text{if } \epsilon \leq \frac{\sigma_{y0}}{E} \\ \frac{\exp\left(-\frac{(\sigma^m - c)^2}{2S_{\text{noise}}^2}\right)}{\left|1 + \frac{Hn}{E}\left(\epsilon - \frac{\sigma_{y0}}{E}\right)^{n-1}\right|} & \text{if } \epsilon > \frac{\sigma_{y0}}{E} \end{cases}, \quad (63)$$

where  $c$  is the value of the theoretical stress when  $\sigma(\epsilon, \mathbf{x}) - w = 0$  is solved for  $\sigma(\epsilon, \mathbf{x})$ . Choosing the prior distribution in the form of a modified normal distribution as:

$$\pi(\mathbf{x}) \propto \begin{cases} \exp\left(-\frac{(\mathbf{x}-\bar{\mathbf{x}})^T \mathbf{\Gamma}_{\mathbf{x}}^{-1}(\mathbf{x}-\bar{\mathbf{x}})}{2}\right) & \text{if } E \geq 0 \text{ and } \sigma_{y0} \geq 0 \text{ and } H \geq 0 \text{ and } n \geq 0 \\ 0 & \text{otherwise} \end{cases}. \quad (64)$$

The final form of the posterior distribution reads:

$$\pi(\mathbf{x}|\boldsymbol{\sigma}^m) \propto \exp\left(-\frac{(\mathbf{x}-\bar{\mathbf{x}})^T \mathbf{\Gamma}_{\mathbf{x}}^{-1}(\mathbf{x}-\bar{\mathbf{x}})}{2}\right) \prod_{i=1}^k \pi(\sigma_i^m|\mathbf{x}), \quad (65)$$

where  $\pi(\sigma_i^m|\mathbf{x})$  must be calculated according to Eq. (63) for each measurement. To investigate the posterior, first  $\sigma(\epsilon, \mathbf{x}) - w = 0$  is numerically solved for  $\sigma(\epsilon, \mathbf{x})$  and then the adaptive MCMC is employed to find the statistical characteristics of the posterior.

#### 4. Bayesian inference for tensile tests with noise in both stress and strain

All the cases studied in section 3 consider an error in the stress, but not in the strain. Both the measured stresses and the measured strains may be polluted by statistical errors however. Both statistical errors are not related to each other, as the devices to measure the forces and strains are independent of each other (e.g. when a load cell and digital image correlation are used). This section deals with the same four material models as in the previous sections but considers that the stresses as well as the strains are influenced by noise.

##### 4.1. Noise distribution

The first calibration experiment is again performed without the use of a specimen. The stress-strain measurements of this test are shown in Fig. 2(a). The measurements in Fig. 2(a) indicate a normal distribution with a zero mean and a diagonal covariance  $\mathbf{\Gamma}_{\text{noise}}$ . The noise model and the evolution of the noise distribution are again investigated by performing a tensile test on a calibration specimen with an exactly known Young's modulus. The schematic results are shown in Fig. 2(b). It is clearly visible that the mean stress and strain values follow a linear, theoretical stress-strain relationship and hence, the covariance does not change. The calibration results show that the additive noise model can also be used in this section.

##### 4.2. Linear elastic

The additive noise model when both the stresses and strains are contaminated by stochastic noise, can be expressed as follows for the linear elastic model:

$$\begin{cases} \sigma^m = E\epsilon + \Omega_\sigma \\ \epsilon^m = \epsilon + \Omega_\epsilon \end{cases}, \quad (66)$$

where  $\sigma^m$  is the measured stress,  $\epsilon^m$  is the measured strain,  $\Omega_\sigma$  is the stochastic error of the stress measurement and  $\Omega_\epsilon$  is the stochastic error of the strain measurement. Because the information from both the measured stress and the measured strain is used here, Bayes' formula for multiple variables must be employed [48]:

$$\pi(E|\sigma^m, \epsilon^m) = \frac{\pi(E)\pi(\epsilon^m|E)\pi(\sigma^m|E, \epsilon^m)}{\pi(\epsilon^m)\pi(\sigma^m|\epsilon^m)}. \quad (67)$$

Since the measured strain and the Young's modulus are statistically independent (measuring a specific strain does not interfere with the probability that a certain Young's modulus occurs, i.e.  $\pi(\epsilon^m|E) = \pi(\epsilon^m)$ ), Eq. (67) can be written as follows:

$$\pi(E|\sigma^m, \epsilon^m) = \frac{\pi(E)\pi(\sigma^m|E, \epsilon^m)}{\pi(\sigma^m|\epsilon^m)}, \quad (68)$$

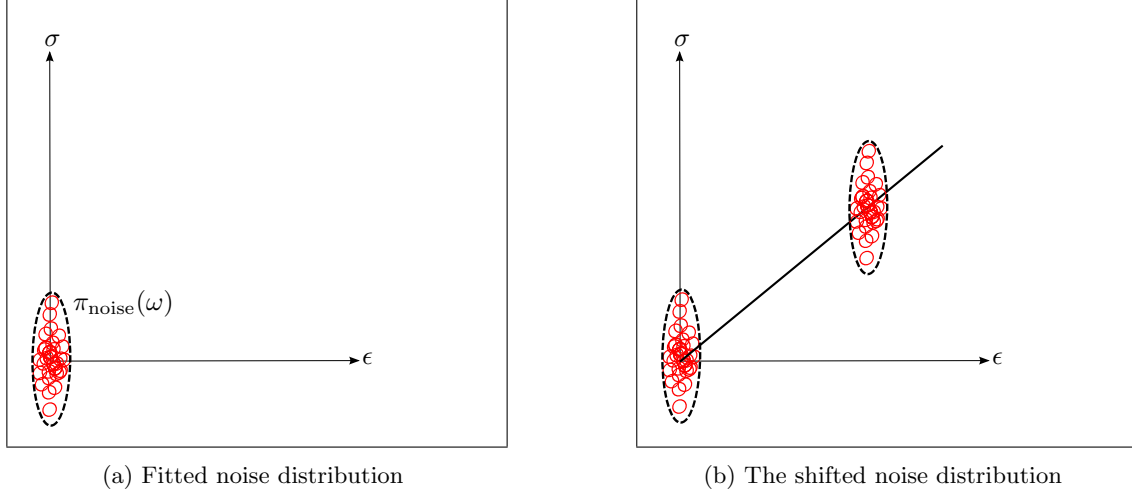


Figure 2: Schematic of the stress-strain measurements (red circles) of the ‘calibration experiments’ for the case with uncertainty in both stress and strain, including some isolines of the noise distributions (dashed). The theoretical stress-strain relation (which is exact for the calibration experiments) is presented as the bold straight line on the diagram on the right.

or, when one is only interested in relative probabilities, as:

$$\pi(E|\sigma^m, \epsilon^m) \propto \pi(E)\pi(\sigma^m|E, \epsilon^m). \quad (69)$$

The issue with Eq. (69) is that the likelihood function,  $\pi(\sigma^m|E, \epsilon^m)$ , must again be determined by integration (over  $\epsilon$  here [46]), because  $\pi(\sigma^m|E, \epsilon)$  can be determined directly, but  $\pi(\sigma^m|E, \epsilon^m)$  not. To this end, we write:

$$\pi(\sigma^m|E, \epsilon^m) = \int_0^a \pi(\sigma^m|E, \epsilon)\pi(\epsilon|\epsilon^m)d\epsilon, \quad (70)$$

where  $a$  is defined by the physical upper bound of the tensile tester (i.e. the ratio of the original length of the specimen and the maximum distance that the clamps can move). Based on Eq. (66) one can express the conditional probabilities  $\pi(\sigma^m|E, \epsilon)$  and  $\pi(\epsilon|\epsilon^m)$  as follows:

$$\begin{cases} \pi(\sigma^m|E, \epsilon) = \pi_{\Omega_\sigma}(\sigma^m - E\epsilon) \\ \pi(\epsilon|\epsilon^m) = \pi_{\Omega_\epsilon}(\epsilon^m - \epsilon) \end{cases}, \quad (71)$$

where  $\pi_{\Omega_\sigma(\omega_\sigma)}$  and  $\pi_{\Omega_\epsilon(\omega_\epsilon)}$  are the noise distributions of the errors in the stress measurements and the strain measurements, respectively. Based on the calibration results in the previous subsection, the noise distribution is a two-dimensional normal distribution with no correlation between the noise in the stress measurements and the noise in the strain measurements (diagonal covariance matrix) and zero mean value as follows:

$$\pi_{\text{noise}}(\boldsymbol{\omega}) = \frac{1}{2\pi\sqrt{|\boldsymbol{\Gamma}_{\text{noise}}|}} \exp\left(-\frac{\boldsymbol{\omega}^T \boldsymbol{\Gamma}_{\text{noise}}^{-1} \boldsymbol{\omega}}{2}\right), \quad (72)$$

where  $\boldsymbol{\omega} = [\omega_\sigma \ \omega_\epsilon]^T$  is the noise vector and  $\boldsymbol{\Gamma}_{\text{noise}}$  is the covariance matrix of the noise distribution in the following form:

$$\begin{bmatrix} S_\sigma^2 & 0 \\ 0 & S_\epsilon^2 \end{bmatrix}, \quad (73)$$

Combining Eqs. (71) and (72), the following two conditional probabilities are required to construct the likelihood function (Eq. (70)):

$$\begin{cases} \pi(\sigma^m|E, \epsilon) = \frac{1}{\sqrt{2\pi}S_\sigma} \exp\left(-\frac{(\sigma^m - E\epsilon)^2}{2S_\sigma^2}\right) \\ \pi(\epsilon|\epsilon^m) = \frac{1}{\sqrt{2\pi}S_\epsilon} \exp\left(-\frac{(\epsilon^m - \epsilon)^2}{2S_\epsilon^2}\right) \end{cases}, \quad (74)$$

Substitution of Eq. (74) in Eq. (70) then results in the following expression for the likelihood function:

$$\pi(\sigma^m|E, \epsilon^m) = \frac{1}{2\pi S_\sigma S_\epsilon} \int_0^a \exp\left(-\left[\frac{(\sigma^m - E\epsilon)^2}{2S_\sigma^2} + \frac{(\epsilon^m - \epsilon)^2}{2S_\epsilon^2}\right]\right) d\epsilon. \quad (75)$$

The result of this integral can be expressed analytically as:

$$\pi(\sigma^m|E, \epsilon^m) = \frac{\sqrt{p_3}}{2\sqrt{2\pi}S_\sigma S_\epsilon} \exp\left(-\frac{p_2 - p_1^2}{2p_3}\right) \left[ \operatorname{erf}\left(\frac{a - p_1}{\sqrt{2p_3}}\right) - \operatorname{erf}\left(\frac{-p_1}{\sqrt{2p_3}}\right) \right], \quad (76)$$

where  $p_1$ ,  $p_2$  and  $p_3$  are formulated as follows:

$$p_1 = \frac{E\sigma^m S_\epsilon^2 + S_\sigma^2 \epsilon^m}{E^2 S_\epsilon^2 + S_\sigma^2}, \quad p_2 = \frac{S_\sigma^2 (\epsilon^m)^2 + S_\epsilon^2 (\sigma^m)^2}{E^2 S_\epsilon^2 + S_\sigma^2}, \quad p_3 = \frac{(S_\sigma S_\epsilon)^2}{E^2 S_\epsilon^2 + S_\sigma^2}. \quad (77)$$

Consequently, choosing the same prior as in Eq. (43), the posterior distribution for  $k$  measurements reads:

$$\pi(E|\sigma^m, \epsilon^m) \propto \exp\left(\frac{(E - \bar{E})^2}{2S_E^2}\right) \left(\frac{\sqrt{p_3}}{2\sqrt{2\pi}S_\sigma S_\epsilon}\right)^k \prod_{i=1}^k \exp\left(-\frac{(p_{2i} - p_{1i}^2)}{2p_3}\right) \left[ \operatorname{erf}\left(\frac{a - p_{1i}}{\sqrt{2p_3}}\right) - \operatorname{erf}\left(\frac{-p_{1i}}{\sqrt{2p_3}}\right) \right], \quad (78)$$

where  $\pi(E|\sigma^m, \epsilon^m) = \pi(E|(\sigma_1^m, \epsilon_1^m), (\sigma_2^m, \epsilon_2^m), \dots, (\sigma_k^m, \epsilon_k^m))$ .

#### 4.3. Linear elastic-perfectly plastic

In case the experimental devices remain the same, but the linear elastic-perfectly plastic model is used, the additive noise model reads:

$$\begin{cases} \sigma^m = \sigma(\epsilon, \mathbf{x}) + \Omega_\sigma \\ \epsilon^m = \epsilon + \Omega_\epsilon \end{cases} \quad (79)$$

where  $\sigma(\epsilon, \mathbf{x})$  is given by Eq. (17) and  $\mathbf{x} = [E \quad \sigma_{y0}]^T$ . For the same noise distribution as in Eq. (72), the conditional probabilities required to construct the likelihood function (Eq. (70)) are:

$$\begin{cases} \pi(\sigma^m|E, \epsilon) = \frac{1}{\sqrt{2\pi}S_\sigma} \exp\left(-\frac{\left(\sigma^m - E\epsilon \left(1 - h\left(\epsilon - \frac{\sigma_{y0}}{E}\right)\right) - \sigma_{y0} h\left(\epsilon - \frac{\sigma_{y0}}{E}\right)\right)^2}{2S_\sigma^2}\right) \\ \pi(\epsilon|\epsilon^m) = \frac{1}{\sqrt{2\pi}S_\epsilon} \exp\left(-\frac{(\epsilon^m - \epsilon)^2}{2S_\epsilon^2}\right) \end{cases}. \quad (80)$$

Combining Eqs. (70) and (80) the likelihood function can be written as:

$$\begin{aligned} \pi(\sigma^m|\mathbf{x}, \epsilon^m) = \frac{1}{2\sqrt{2\pi}S_\epsilon S_\sigma} & \left( \sqrt{p_3} \exp\left(-\frac{p_2 - p_1^2}{2p_3}\right) \left[ \operatorname{erf}\left(\frac{\frac{\sigma_{y0}}{E} - p_1}{\sqrt{2p_3}}\right) - \operatorname{erf}\left(\frac{-p_1}{\sqrt{2p_3}}\right) \right] + \right. \\ & \left. S_\epsilon \exp\left(-\frac{(\sigma^m - \sigma_{y0})^2}{2S_\sigma^2}\right) \left[ \operatorname{erf}\left(\frac{\epsilon^m - \frac{\sigma_{y0}}{E}}{\sqrt{2}S_\epsilon}\right) - \operatorname{erf}\left(\frac{\epsilon^m - a}{\sqrt{2}S_\sigma}\right) \right] \right). \quad (81) \end{aligned}$$

where  $p_1$ ,  $p_2$  and  $p_3$  again given by Eq. (77). Finally, selecting the prior distribution as in Eq. (51), the posterior distribution for  $k$  measurements reads:

$$\pi(\mathbf{x}|\boldsymbol{\sigma}^m, \boldsymbol{\epsilon}^m) \propto \exp\left(\frac{(\mathbf{x} - \bar{\mathbf{x}})^T \boldsymbol{\Gamma}_{\mathbf{x}}^{-1} (\mathbf{x} - \bar{\mathbf{x}})}{2}\right) \prod_{i=1}^k \pi(\sigma_i^m | \mathbf{x}, \epsilon_i^m). \quad (82)$$

#### 4.4. Linear elastic-linear hardening

For the linear elastic-linear hardening model, the unknown parameters are  $\mathbf{x} = [E \ \sigma_{y0} \ H]^T$ . Assuming the same experimental equipment as in subsections 4.2 and 4.3 and employing Eqs. (20) and (70), the likelihood function can be expressed as:

$$\begin{aligned} \pi(\sigma^m | \mathbf{x}, \epsilon^m) = & \frac{1}{2\sqrt{2\pi} S_\sigma S_\epsilon} \left( \sqrt{p_3} \exp\left(-\frac{p_2 - p_1^2}{2p_3}\right) \left[ \operatorname{erf}\left(\frac{\frac{\sigma_{y0}}{E} - p_1}{\sqrt{2p_3}}\right) - \operatorname{erf}\left(\frac{-p_1}{\sqrt{2p_3}}\right) \right] + \right. \\ & \left. \frac{1}{\sqrt{\beta_1}} \exp\left(-\frac{\beta_1 \beta_3 - \beta_2^2}{2\beta_1}\right) \left[ \operatorname{erf}\left(\frac{\sqrt{\beta_1} a - \frac{\beta_2}{\sqrt{\beta_1}}}{\sqrt{2}}\right) - \operatorname{erf}\left(\frac{\frac{\sigma_{y0} \sqrt{\beta_1}}{E} - \frac{\beta_2}{\sqrt{\beta_1}}}{\sqrt{2}}\right) \right] \right), \end{aligned} \quad (83)$$

where  $p_1$ ,  $p_2$  and  $p_3$  are again given by Eq. (77) and  $\beta_1$ ,  $\beta_2$  and  $\beta_3$  are determined as follows:

$$\begin{aligned} \beta_1 = & \frac{\left(\frac{HE}{H+E}\right)^2}{S_\sigma^2} + \frac{1}{S_\epsilon^2}, \quad \beta_2 = \frac{(\sigma^m - \sigma_{y0}) \frac{HE}{H+E} + \left(\frac{HE}{H+E}\right)^2 \frac{\sigma_{y0}}{E}}{S_\sigma^2} + \frac{\epsilon^m}{S_\epsilon^2}, \\ \beta_3 = & \frac{(\sigma^m - \sigma_{y0})^2 + 2(\sigma^m - \sigma_{y0}) \frac{HE}{H+E} \frac{\sigma_{y0}}{E} + \left(\frac{HE}{H+E}\right)^2 \left(\frac{\sigma_{y0}}{E}\right)^2}{S_\sigma^2} + \frac{(\epsilon^m)^2}{S_\epsilon^2}. \end{aligned} \quad (84)$$

Selecting the same posterior distribution as in Eq. (54), the posterior distribution is again of the following form:

$$\pi(\mathbf{x}|\boldsymbol{\sigma}^m, \boldsymbol{\epsilon}^m) \propto \exp\left(\frac{(\mathbf{x} - \bar{\mathbf{x}})^T \boldsymbol{\Gamma}_{\mathbf{x}}^{-1} (\mathbf{x} - \bar{\mathbf{x}})}{2}\right) \prod_{i=1}^k \pi(\sigma_i^m | \mathbf{x}, \epsilon_i^m). \quad (85)$$

where  $\pi(\sigma_i^m | \mathbf{x}, \epsilon_i^m)$  is calculated using Eq. (83) for each pair of measurements  $(\sigma_i^m, \epsilon_i^m)$ .

#### 4.5. Linear elastic-nonlinear hardening

Like in subsection 3.5 the parameter vector for the current case reads  $\mathbf{x} = [E \ \sigma_{y0} \ H \ n]^T$ . As the experimental equipment remains the same, the additive noise model is still valid and hence, the following expressions for the measured stresses and strains are employed:

$$\begin{cases} \sigma^m = \sigma(\mathbf{x}, \epsilon) + \Omega_\sigma \\ \epsilon^m = \epsilon + \Omega_\epsilon \end{cases}. \quad (86)$$

In contrast to the previous models in this subsection, the theoretical stress ( $\sigma(\mathbf{x}, \epsilon)$  in the first equation of Eq. (86)) is an implicit function (Eq. (23)) and as a result the construction of the likelihood function differs. First, Eq. (86) is rewritten using Eq. (23):

$$\begin{cases} \sigma^m = E \epsilon \left(1 - h\left(\epsilon - \frac{\sigma_{y0}}{E}\right)\right) + \left(\sigma_{y0} + H \left(\epsilon - \frac{\sigma_{y0}}{E}\right)^n\right) h\left(\epsilon - \frac{\sigma_{y0}}{E}\right) + \Omega_\sigma \\ \epsilon^m = \epsilon + \Omega_\epsilon \end{cases}, \quad (87)$$

from which it is clear that the measured stress is not only a function of the material parameters ( $\mathbf{x}$ ) and the theoretical strain ( $\epsilon$ ) but also of the theoretical stress ( $\sigma(\mathbf{x}, \epsilon)$ ).

The following conditional probabilities for the measured stress and measured strain are established:

$$\begin{cases} \pi(\sigma^m | \mathbf{x}, \epsilon, \sigma(\mathbf{x}, \epsilon)) = \pi_{\Omega_\sigma}(\sigma^m - \sigma(\mathbf{x}, \epsilon)) \\ \pi(\epsilon | \epsilon^m) = \pi_{\Omega_\epsilon}(\epsilon^m - \epsilon) \end{cases}. \quad (88)$$

The required likelihood function then reads:

$$\pi(\sigma^m | \mathbf{x}, \epsilon^m) = \int_0^a \int_0^{+\infty} \pi(\sigma^m | \mathbf{x}, \epsilon, \sigma(\mathbf{x}, \epsilon)) \pi(\sigma(\mathbf{x}, \epsilon) | \mathbf{x}, \epsilon) \pi(\epsilon | \epsilon^m) d\sigma d\epsilon, \quad (89)$$

where  $\pi(\sigma^m | \mathbf{x}, \epsilon, \sigma(\mathbf{x}, \epsilon))$  and  $\pi(\epsilon | \epsilon^m)$  are given by Eq. (88). If the material parameters and the theoretical strain are given, the conditional probability  $\pi(\sigma(\mathbf{x}, \epsilon) | \mathbf{x}, \epsilon)$  reads:

$$\pi(\sigma(\mathbf{x}, \epsilon) | \mathbf{x}, \epsilon) = \delta(\sigma(\mathbf{x}, \epsilon) - w), \quad (90)$$

where  $w$  is again used to abbreviate the right hand side of Eq. (23). Consequently, the resulting likelihood function reads:

$$\begin{aligned} \pi(\sigma^m | \mathbf{x}, \epsilon^m) = \frac{1}{2\pi S_\sigma S_\epsilon} \int_0^a \int_0^{+\infty} & \delta(\sigma(\mathbf{x}, \epsilon) - w) \exp\left(-\frac{(\epsilon^m - \epsilon)^2}{2S_\epsilon^2}\right) \\ & - \frac{\left(\sigma^m - E\epsilon\left(1 - h\left(\epsilon - \frac{\sigma_{y0}}{E}\right)\right) - \left(\sigma_{y0} + H\left(\epsilon - \frac{\sigma(\mathbf{x}, \epsilon)}{E}\right)^n\right)h\left(\epsilon - \frac{\sigma_{y0}}{E}\right)\right)^2}{2S_{\sigma^2}} d\sigma d\epsilon. \end{aligned} \quad (91)$$

This can furthermore be expressed as:

$$\pi(\sigma^m | \mathbf{x}, \epsilon^m) = \frac{1}{2\pi S_\sigma S_\epsilon} (I_1 + I_2), \quad (92)$$

where

$$I_1 = \int_0^{\frac{\sigma_{y0}}{E}} \int_0^{+\infty} \delta(\sigma(\mathbf{x}, \epsilon) - w) \exp\left(-\frac{(\epsilon^m - \epsilon)^2}{2S_\epsilon^2} - \frac{(\sigma^m - E\epsilon)^2}{2S_{\sigma^2}}\right) d\sigma d\epsilon, \quad (93)$$

and

$$I_2 = \int_{\frac{\sigma_{y0}}{E}}^a \int_0^{+\infty} \delta(\sigma(\mathbf{x}, \epsilon) - w) \exp\left(-\frac{(\epsilon^m - \epsilon)^2}{2S_\epsilon^2} - \frac{\left(\sigma^m - \left(\sigma_{y0} + H\left(\epsilon - \frac{\sigma(\mathbf{x}, \epsilon)}{E}\right)^n\right)h\left(\epsilon - \frac{\sigma_{y0}}{E}\right)\right)^2}{2S_{\sigma^2}}\right) d\sigma d\epsilon. \quad (94)$$

Using the Dirac delta function properties and Eq. (62),  $I_1$  equals to:

$$I_1 = \frac{\sqrt{\pi p_3}}{\sqrt{2}} \exp\left(-\frac{p_2 - p_1^2}{2p_3}\right) \left[ \operatorname{erf}\left(\frac{\frac{\sigma_{y0}}{E} - p_1}{\sqrt{2p_3}}\right) - \operatorname{erf}\left(\frac{-p_1}{\sqrt{2p_3}}\right) \right], \quad (95)$$

where  $p_1$ ,  $p_2$  and  $p_3$  are given by Eq. (77). To calculate  $I_2$ , one first needs to find the solution for  $g(z)$  in Eq. (62), for which it must be substituted by  $w$ . Again using the Dirac delta function properties and integrating Eq. (94) over the theoretical stress,  $I_2$  reads:

$$I_2 = \int_{\frac{\sigma_{y0}}{E}}^a \exp\left(-\frac{(\epsilon^m - \epsilon)^2}{2S_\epsilon^2} - \frac{\left(\sigma^m - \left(\sigma_{y0} + H\left(\epsilon - \frac{w}{E}\right)^n\right)\right)^2}{2S_\sigma^2}\right) \frac{1}{\left|1 + \frac{Hn}{E}\left(\epsilon - \frac{w}{E}\right)^{n-1}\right|} d\epsilon, \quad (96)$$

which can be calculated by numerical approaches (e.g. Simpson's rule). Finally for the same prior distribution as in Eq. (64), the posterior distribution for  $k$  observations becomes:

$$\pi(\mathbf{x}|\boldsymbol{\sigma}^m, \boldsymbol{\epsilon}^m) \propto \exp\left(\frac{(\mathbf{x} - \bar{\mathbf{x}})^T \boldsymbol{\Gamma}_{\mathbf{x}}^{-1} (\mathbf{x} - \bar{\mathbf{x}})}{2}\right) \prod_{i=1}^k \pi(\sigma_i^m | \mathbf{x}, \epsilon_i^m). \quad (97)$$

Note that in practice once a sample is drawn by the adaptive MCMC approach, the integral in Eq. (97) and subsequently the likelihood function can be calculated.

## 5. Examples

All formulations derived in the previous two section are investigated in this section. The effect of the prior distribution on the posterior distribution is studied, as well as BI's ability to recover a material parameter distribution when they are taken from a specific distribution. Also, BI's ability to recover correlations between different material parameters is exposed.

### 5.1. Bayesian inference with noise in stress

This subsection presents several examples for the BI formulations of section 3, in which only a statistical noise in the stress measurements is considered.

#### 5.1.1. Linear elastic (LE)

In the first example a specimen with a Young's modulus of 210 GPa is considered, which is to be identified. 'Calibration experiments' were performed and the noise in the stress follows the normal distribution of Eq. (40) with  $S_{\text{noise}} = 0.01$  GPa. For only one stress measurement  $\sigma^m = 0.1576$  GPa with a corresponding strain  $\epsilon = 7.25 \times 10^{-4}$ , the posterior distribution is calculated using Eq. (46). Selecting the prior distribution as in Eq. (43) with mean  $\bar{E} = 150$  GPa and relatively large standard deviation  $S_E = 50$  GPa, the posterior reads:

$$\pi(E|\sigma^m) \propto \exp\left(-\frac{(E - \mu_{\text{post}})^2}{2S_{\text{post}}^2}\right), \quad E \geq 0, \quad (98)$$

where  $\mu_{\text{post}} = 212.6486$  GPa and  $S_{\text{post}} = 13.2964$  GPa.

Fig. 3 shows this posterior distribution, as well as the prior distribution and the value predicted by the least squares method when one measurement is made and also when five measurements are made. Fig. 4 presents the linear elastic responses for the case when one measurement is made and for the case when ten measurements are made. The figure also shows the stress-strain responses made with Young's moduli taken within the 95% credible region of the posterior.

Two issues can be observed based on Fig. 3. First, the strain at which a measurement is made has a profound influence on the posterior. This can be observed when the posterior of Fig. 3(a) is compared to the posterior of Fig. 3(b) when only the first measurement is incorporated (the distribution denoted by  $\pi(E|\sigma_1^m)$ ). The latter distribution is significantly wider and its MAP point is relatively far away from the specimen's Young's modulus. Hence, a measurement made at a comparatively large strain reduces the width of the posterior distribution (i.e. the uncertainty reduces).

The second issue to be observed is that for an increasing number of measurements, the posterior becomes narrower and the MAP point moves closer to the specimen's Young's modulus.

When the MAP point ( $\mu_{\text{post}} = 207.2821$  GPa) for a single measurement is compared with the result of the least squares method for the same measurement ( $E_{\text{ls}} = 210.2216$  GPa), one can notice the effect of the selected prior distribution. One may therefore think that the least squares method gives a more accurate result than BI (although this depends the selected prior). After all, the result of the least squares method is closer to the specimen's Young's modulus than the MAP point determined using BI. On the other hand, one can make the point that the result determined using the least squares method is not the actual Young's modulus of the specimen (210 GPa), whereas the posterior distribution of BI does include this value. The

main issue is however that BI cannot truly be compared to the least squares method, because it considers the Young's modulus to be stochastic of nature. This means that BI accounts for the fact that it originates from a distribution (for which the user is required to give a hunch, which is reflected in the prior). In the least squares method the Young's modulus is a deterministic value, which can only be determined using the current measurements. Hence, it does not consider that if other measurements would be made (due to different noise realisations), the resulting Young's modulus would differ.

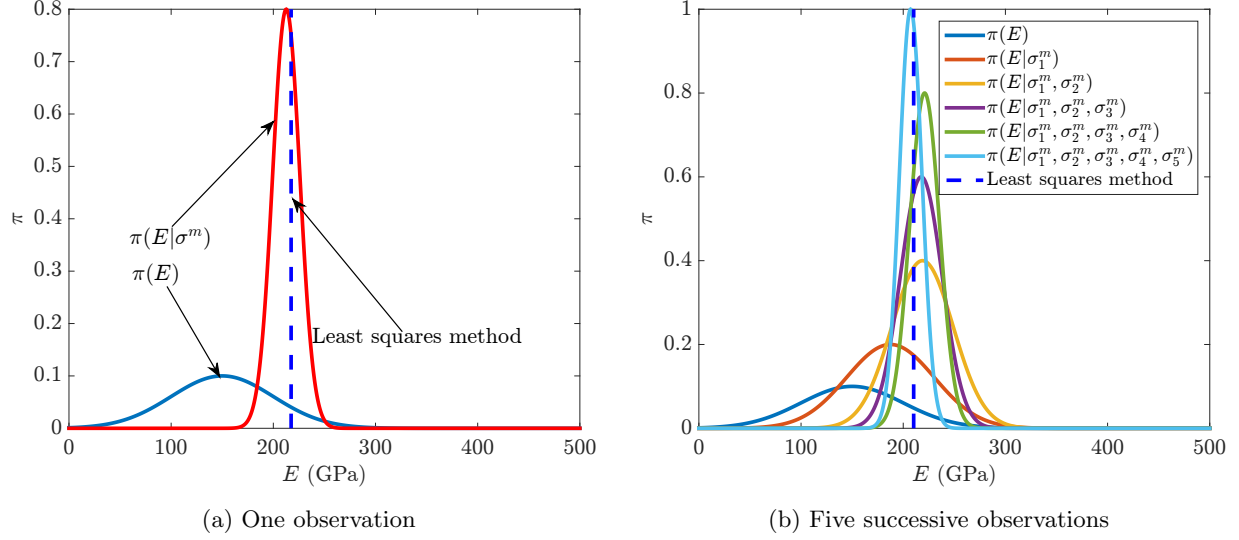


Figure 3: LE: The prior, the posterior and the value predicted by least squares method. The distributions are not normalised. The strain at which a measurement is made has a considerable influence on the posterior. This can be observed when the posterior of (a) ( $\pi(E|\sigma^m)$ , red line) is compared to the posterior of (b) when only the first measurement is incorporated ( $\pi(E|\sigma_1^m)$ , red line). Left: an increase of the number of measurements leads to narrow posteriors with their MAP estimates closer to the specimen's Young's modulus.



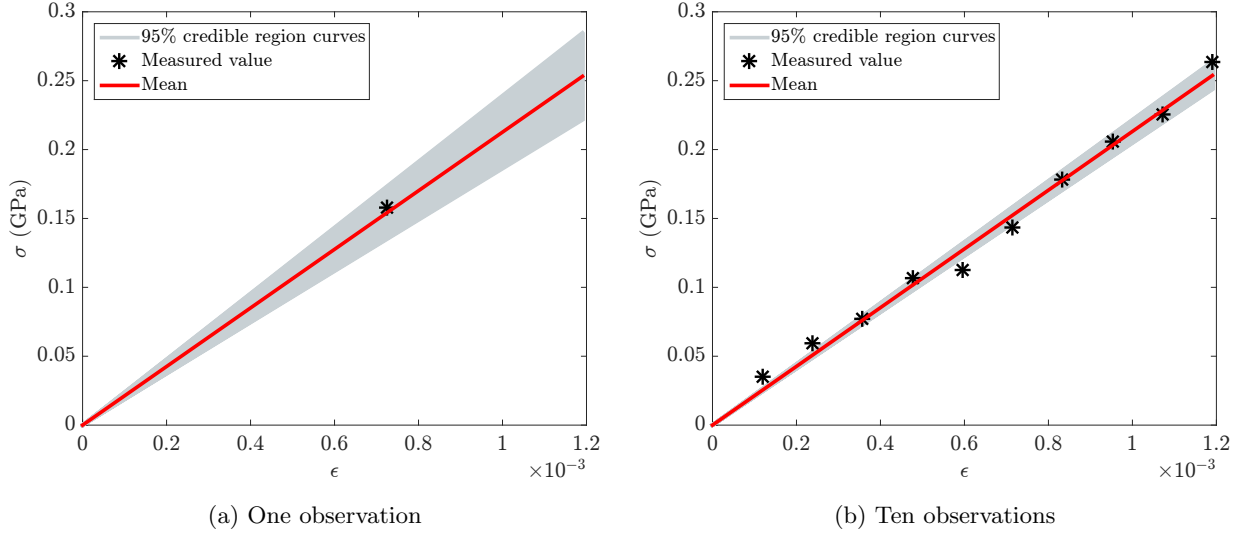


Figure 4: LE: The measurements, and the stress-strain curves created using the posterior for (a) one measurement and (b) ten measurements. Increasing the number of measurements leads to a narrower posterior distribution 95% credible region.

It is nevertheless interesting to study the effect of the prior distribution on the MAP point (which is the same as the mean value for the normal posteriors in this subsection). In Fig. 5 the MAP points are shown as a function of the mean and the standard deviation of the prior. The MAP points are presented for different numbers of measurements. As can be seen, an increasing the number of measurements leads to a flatter surface, which means that the influence of the prior distribution decreases.

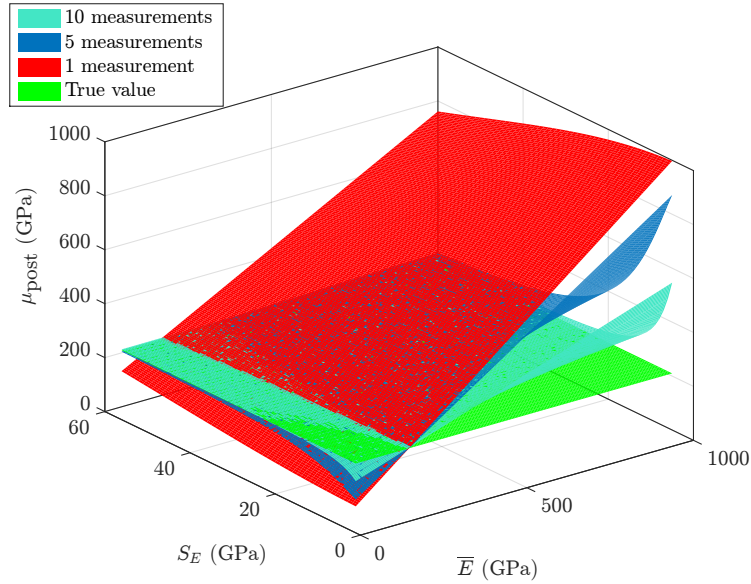


Figure 5: LE: The influence of the prior (i.e. the mean value and the standard deviation) on the resulting MAP point for different numbers of successive measurements. Increasing the number of the measurements leads to a flatter surface which indicates a decreasing influence of the prior distribution.

A last important issue to show using the linear elastic model is BI's ability (or inability for the current formulation) to capture the heterogeneity of the material parameters. The question here is thus if BI is able to recover the distribution of the Young's modulus when multiple specimens are tested and their Young's moduli are taken from a specific distribution. To this end, 25 specimens are considered of which the Young's moduli are taken from a normal distribution with a mean value of 210 GPa and a standard deviation of 10 GPa (blue curve in Fig. 6). Of each specimen ten measurements are made. The same noise model and noise distribution are applied.

The resulting posterior is presented by the red line in Fig. 6, which is a (modified) normal distribution with  $\mu_{\text{post}} = 215.3971$  GPa and  $S_{\text{post}} = 0.8561$  GPa. The posterior is substantially narrower than the distribution of the specimens' Young's moduli and hence, using the BI formulations of this contribution, the material heterogeneity cannot be captured. This entails that the width of the posterior distributions (represented by  $S_{\text{post}}$  in this subsection) is only a measure for the uncertainty of the MAP points and the mean value and not for the material heterogeneity.

To be able to recover the material heterogeneity one needs to consider both the inherent uncertainty of the material parameters as well as that of the measurements. This means that in that case, one does not only aim to determine the posterior of the material parameter(s), but also the posterior of the variance of the assumed material parameter distribution. Our future work will focus on this.

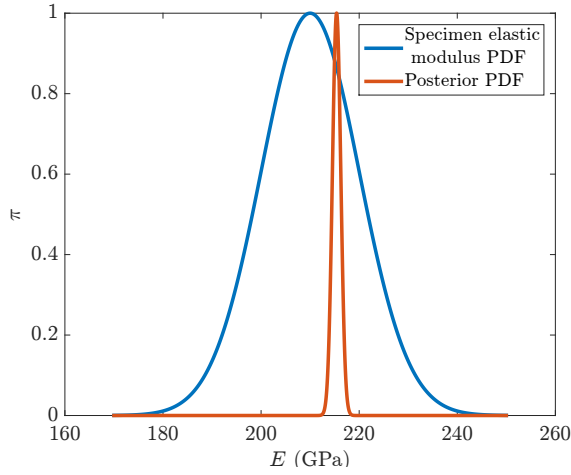


Figure 6: LE: The distribution of the specimens' Young's moduli and the resulting posterior. The PDFs are not normalised. The current formulation is clearly not able to recover the material heterogeneity. To be able to recover the material heterogeneity one needs to consider both the inherent uncertainty of the material parameters as well as that of the measurements.

#### 5.1.2. Linear elastic-perfectly plastic (LE-PP)

In the first example of this subsection one specimen is considered with a Young's modulus  $E = 210$  GPa and an initial yield stress  $\sigma_{y0} = 0.25$  GPa. Twelve measurements are generated by employing the same noise distribution as in the previous subsection. The prior distribution of Eq. (51) is furthermore selected with the following mean vector and covariance matrix:

$$\bar{\mathbf{x}} = \begin{bmatrix} 200 \\ 0.29 \end{bmatrix} \text{ GPa}, \quad \mathbf{\Gamma}_{\mathbf{x}} = \begin{bmatrix} 2500 & 0 \\ 0 & 2.7778 \times 10^{-4} \end{bmatrix} \text{ GPa}^2. \quad (99)$$

Consequently, the posterior for the LE-PP model of subsection 2.2.2 is of the form as presented in Eq. (52), which is investigated by the MCMC approach given in subsection 2.3.2. Running the chain for  $10^4$  samples

yields:

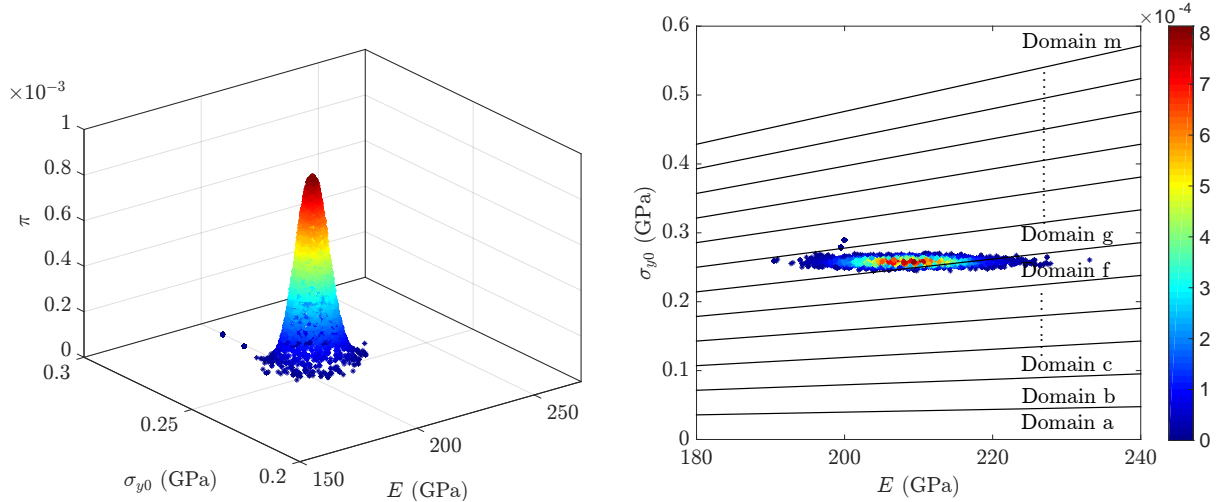
$$\boldsymbol{\mu}_{\text{post}} = \begin{bmatrix} 208.9859 \\ 0.2578 \end{bmatrix} \text{ GPa}, \quad \boldsymbol{\Gamma}_{\text{post}} = \begin{bmatrix} 29.807 & 4.1064 \times 10^{-4} \\ 4.1064 \times 10^{-4} & 1.5067 \times 10^{-5} \end{bmatrix} \text{ GPa}^2. \quad (100)$$

Furthermore, the MAP point equals to:

$$\mathbf{MAP} = \begin{bmatrix} 208.4475 \\ 0.2578 \end{bmatrix} \text{ GPa}. \quad (101)$$

Fig. 7(a) shows the samples generated by the adaptive MCMC approach which are used to approximate the posterior distribution. The domains presented in Fig. 7(b) show which of the measurements are included in the elastic part and which are included in the plastic part. The occurrence of these discrete domains is a result of the  $C_0$ -continuity of Eq. (17). In domain ‘a’ (in which no samples are generated by the adaptive MCMC approach), all the measurements are considered to be in the plastic part. In domain ‘b’ on the other hand, the first measurement (the one with the smallest strain) is considered to be in the elastic part and the others remain considered in the plastic part. Continuing like this, in domain ‘c’ the second measurement is also considered to be in the elastic part. Finally, in domain ‘m’ all measurements are considered to be in the plastic domain. Based on Fig. 7(b) the MAP point is clearly located in the domain in which the first six measurements are considered to be in the elastic part and the remaining in the plastic part.

The 95% credible region is shown together with the posterior distribution in Fig. 8(a). The possible stress-strain responses inside the credible region are presented in Fig. 8(b).



(a) Samples generated by the adaptive MCMC approach (b) Samples generated by the adaptive MCMC approach (top view) including different domains

Figure 7: LE-PP: Two different views of the samples generated by the adaptive MCMC approach to approximate the posterior. The colours represent the value of the posterior, which in the left image is also shown along the z-axis. In Fig. 7(b) several domains are shown. For each of these domains, the measurements considered to be in the elastic part and the measurements considered to be in the plastic part remain the same.

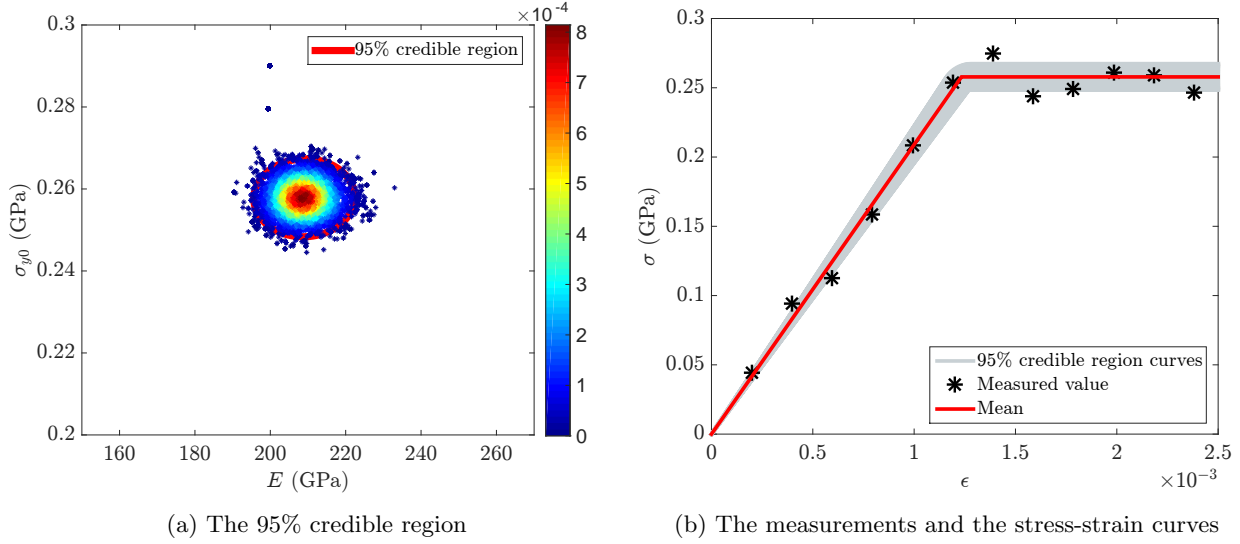


Figure 8: LE-PP: The 95% credible region of the posterior distribution, the measurements and the stress-strain curves created using the posterior. The 95% credible region curves in (b) are plotted using the points inside the 95% credible region marked by red ellipse in (a).

The posterior distribution seems to be roughly of an elliptical shape with the primary axes almost along the  $E$ -axis and  $\sigma_{y0}$ -axis. This entails that the correlation between the two material parameters is not significant. One has to notice though, that the assumed prior is uncorrelated. In other words, the prior covariance matrix ( $\Gamma_{\mathbf{x}}$ ) is diagonal. It is therefore interesting to investigate the influence of the off-diagonal term of the prior covariance matrix on the posterior covariance matrix. In Fig. 9 this influence is graphically presented for the three terms of the posterior covariance matrix (note that both the prior covariance matrix and the posterior covariance matrix are symmetric). It seems that an increase of  $(\Gamma_x)_{12}$  leads to some decreasing trend of  $(\Gamma_{\text{post}})_{11}$  and some increasing trend of  $(\Gamma_{\text{post}})_{12}$ . However, it is difficult to assess whether or not a true trend is present in these results.

The next example focuses on the ability of the current formulation to capture a correlation between the Young's modulus and the initial yield stress when the material parameters of the specimens are correlated. To this end, ten specimens are considered of which the material parameters are governed by a normal distribution with the following mean vector and covariance matrix:

$$\bar{\mathbf{x}}_{\text{spc}} = \begin{bmatrix} 210 \\ 0.25 \end{bmatrix} \text{ GPa}, \quad \Gamma_{\text{spc}} = \begin{bmatrix} 100 & 10^{-4} \\ 10^{-4} & 1.1111 \times 10^{-4} \end{bmatrix} \text{ GPa}^2. \quad (102)$$

For each specimen twelve measurements are made. Using the same prior as in the previous example (see Eq. (99)) and running the adaptive MCMC approach for  $10^4$  samples yields:

$$\boldsymbol{\mu}_{\text{post}} = \begin{bmatrix} 211.1077 \\ 0.2519 \end{bmatrix} \text{ GPa}, \quad \Gamma_{\text{post}} = \begin{bmatrix} 5.5373 & -8.396 \times 10^{-4} \\ -8.396 \times 10^{-4} & 1.8174 \times 10^{-6} \end{bmatrix} \text{ GPa}^2. \quad (103)$$

The MAP estimator is given by:

$$\mathbf{MAP} = \begin{bmatrix} 210.5923 \\ 0.2521 \end{bmatrix} \text{ GPa}. \quad (104)$$

These results show that the correlation of the posterior is not the same as that of the distribution of the actual material. This corresponds closely with the observation that the formulations in this contribution are not able to capture any of the intrinsic uncertainty of the material parameters. Fig. 10 shows the effect of the

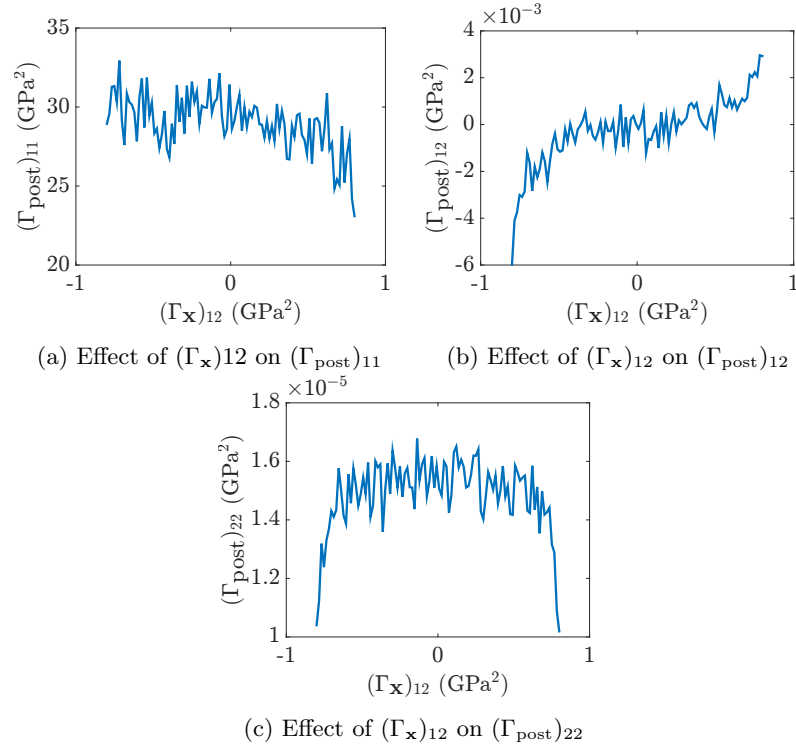


Figure 9: LE-PP: Effect of the off-diagonal component of the prior covariance matrix on the posterior covariance matrix. It seems that an increase of  $(\Gamma_x)_{12}$  leads to some decreasing trend of  $(\Gamma_{\text{post}})_{11}$  and some increasing trend of  $(\Gamma_{\text{post}})_{12}$ . However, it is difficult to assess whether or not a true trend is present in these results.

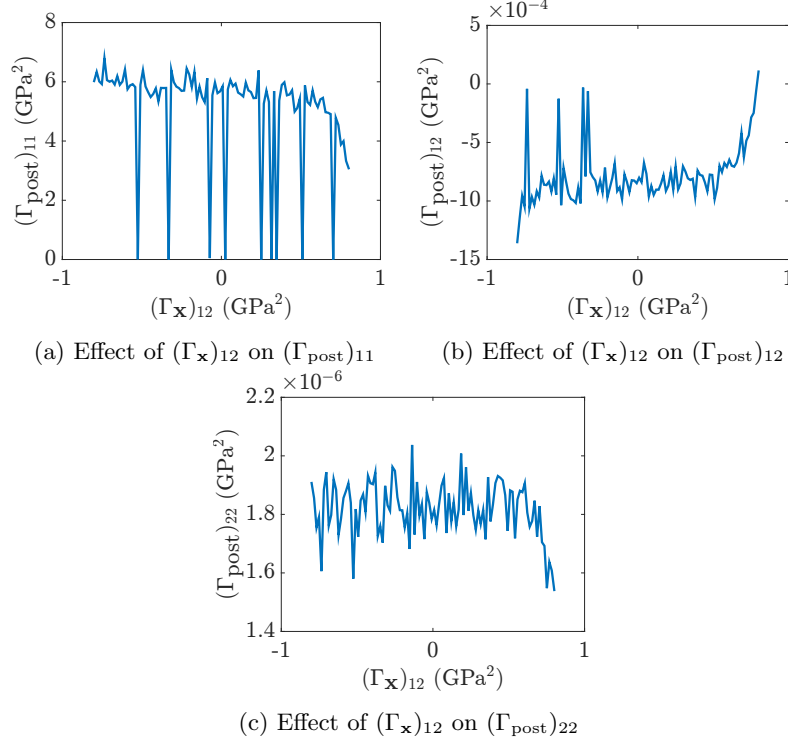


Figure 10: LE-PP: Effect of the off-diagonal components of the prior covariance matrix on the posterior distribution covariance matrix when the measurements are generated from specimens drawn from a normal distribution given in Eq. (102). No real trends can be observed.

off-diagonal component of the prior covariance matrix ( $\Gamma_{\mathbf{x}}$ ) on the components of the posterior covariance matrix ( $\Gamma_{\text{post}}$ ). Again, no real trends can be observed.

In the last example of this subsection, we will regard how the formulation for the linear elastic-perfectly plastic model behaves when it is used for a material that hardens nonlinearly. To this end, fifteen measurements are generated using the linear elastic-nonlinear hardening model with  $E = 210$  GPa,  $\sigma_{y0} = 0.25$  GPa,  $H = 2$  GPa and  $n = 0.5$  and the same noise distribution and noise model as in the previous examples. Employing the prior distribution in the form of Eq. (51) with mean and covariance matrix of Eq. (99) and running the adaptive MCMC approach for  $10^4$  samples leads to:

$$\boldsymbol{\mu}_{\text{post}} = \begin{bmatrix} 206.4357 \\ 0.2941 \end{bmatrix} \text{ GPa}, \quad \Gamma_{\text{post}} = \begin{bmatrix} 31.2818 & -3.0214 \times 10^{-3} \\ -3.0214 \times 10^{-3} & 1.1279 \times 10^{-5} \end{bmatrix} \text{ GPa}^2, \quad (105)$$

and the MAP point for this case reads:

$$\mathbf{MAP} = \begin{bmatrix} 204.8997 \\ 0.2944 \end{bmatrix} \text{ GPa}. \quad (106)$$

The stress-strain curves associated with the 95% credible region in Fig. 11 show that six measurements belong to the elastic part of the response for the MAP estimate.

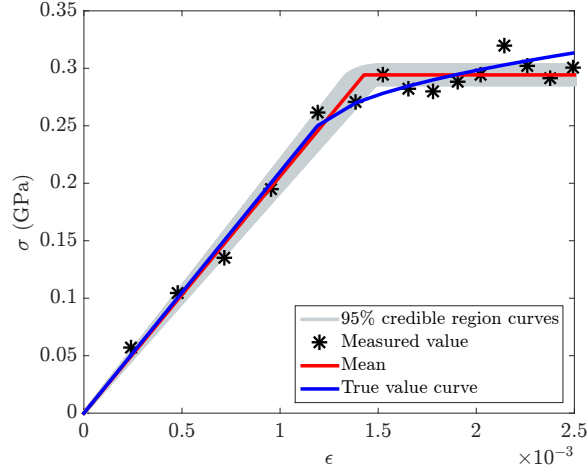


Figure 11: LE-PP: The measurements, the stress-strain curves using  $\mu_{\text{post}}$  including the 95% credible region and the linear elastic-nonlinear hardening curve used to create the measurements.

### 5.1.3. Linear elastic-linear hardening (LE-LH)

This subsection deals with the Bayesian formulation for the linear elastic-linear hardening model. A specimen with a Young's modulus  $E = 210$  GPa, an initial yield stress  $\sigma_{y0} = 0.25$  GPa and a plastic modulus  $H = 50$  GPa is regarded. Twelve measurements are created by employing the same distribution in the stress as in the previous subsection. The prior distribution is given by Eq. (54) with the following properties:

$$\bar{\mathbf{x}} = \begin{bmatrix} 200 \\ 0.29 \\ 60 \end{bmatrix} \text{ GPa}, \quad \mathbf{\Gamma}_{\mathbf{x}} = \begin{bmatrix} 2500 & 0 & 0 \\ 0 & 2.7778 \times 10^{-4} & 0 \\ 0 & 0 & 100 \end{bmatrix} \text{ GPa}^2. \quad (107)$$

Running the adaptive MCMC algorithm for  $10^4$  samples gives:

$$\mu_{\text{post}} = \begin{bmatrix} 207.4586 \\ 0.2533 \\ 55.9187 \end{bmatrix} \text{ GPa}, \quad \mathbf{\Gamma}_{\text{post}} = \begin{bmatrix} 36.5642 & -1.2746 \times 10^{-2} & -3.7886 \\ -1.2746 \times 10^{-2} & 4.0359 \times 10^{-5} & -2.6218 \times 10^{-2} \\ -3.7886 & -2.6218 \times 10^{-2} & 66.8214 \end{bmatrix} \text{ GPa}^2, \quad (108)$$

and

$$\mathbf{MAP} = \begin{bmatrix} 206.9528 \\ 0.2548 \\ 55.2838 \end{bmatrix} \text{ GPa}. \quad (109)$$

Fig. 12 shows the generated samples by the adaptive MCMC approach in the  $E - \sigma_{y0} - H$  space including the projections on the  $E - \sigma_{y0}$ ,  $E - H$  and  $\sigma_{y0} - H$  planes.

The 95% credible region is presented in Fig. 13(a) and the possible stress-strain responses associated with the credible region are shown in Fig. 13(b).

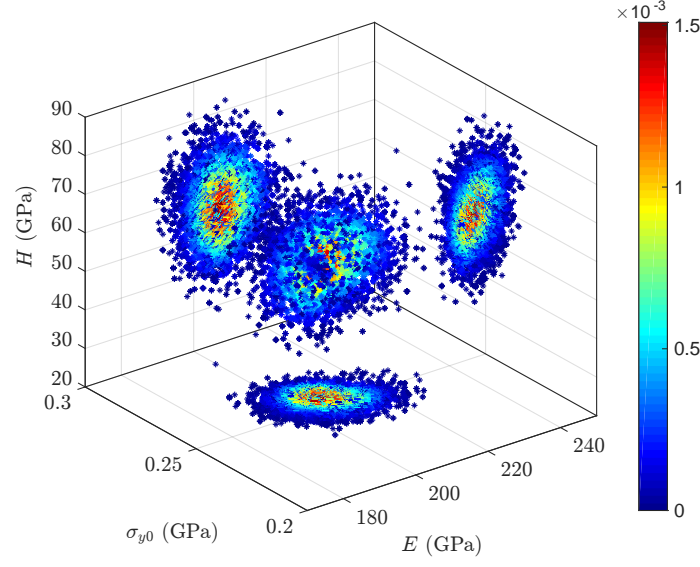
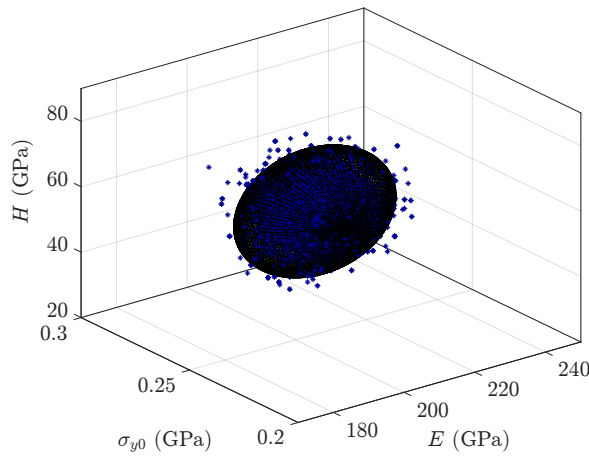
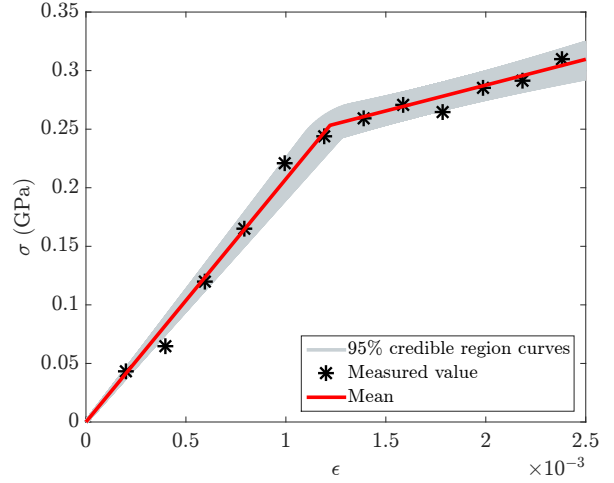


Figure 12: LE-LH: Samples generated by the adaptive MCMC approach to approximate the posterior distribution and its projection on the three planes.



(a) The 95% credible region



(b) The measurements and the stress-strain curves

Figure 13: LE-LH: The 95% credible region of the posterior distribution, the measurements and the stress-strain curves created using the posterior.

#### 5.1.4. Linear elastic-nonlinear hardening (LE-NH)

For this subsection twelve measurements are generated based on a specimen with  $E = 210$  GPa,  $\sigma_{y0} = 0.25$  GPa,  $H = 2$  GPa,  $n = 0.57$  and the same noise distribution as previous subsections. The prior



distribution is selected in the form of Eq. (64) with the following mean vector and covariance matrix:

$$\bar{\mathbf{x}} = \begin{bmatrix} 200 \\ 0.29 \\ 2.5 \\ 0.57 \end{bmatrix} \text{ GPa}, \quad \mathbf{\Gamma}_{\mathbf{x}} = \begin{bmatrix} 2500 & 0 & 0 & 0 \\ 0 & 2.7778 \times 10^{-4} & 0 & 0 \\ 0 & 0 & 0.1111 & 0 \\ 0 & 0 & 0 & 0.0025 \end{bmatrix} \text{ GPa}^2. \quad (110)$$

Running the adaptive MCMC approach for  $10^4$  samples yields:

$$\begin{aligned} \boldsymbol{\mu}_{\text{post}} &= \begin{bmatrix} 209.8035 \\ 0.2566 \\ 2.1602 \\ 0.6034 \end{bmatrix} \text{ GPa}, \\ \mathbf{\Gamma}_{\text{post}} &= \begin{bmatrix} 25.6975 & -3.9287 \times 10^{-3} & -9.0948 \times 10^{-2} & -6.8572 \times 10^{-3} \\ -3.9287 \times 10^{-3} & 7.7856 \times 10^{-5} & -5.2198 \times 10^{-4} & 1.4961 \times 10^{-4} \\ -9.0948 \times 10^{-2} & -5.2198 \times 10^{-4} & 9.6433 \times 10^{-2} & 5.7512 \times 10^{-3} \\ -6.8572 \times 10^{-3} & 1.4961 \times 10^{-4} & 5.7512 \times 10^{-3} & 9.6817 \times 10^{-4} \end{bmatrix} \text{ GPa}^2, \end{aligned} \quad (111)$$

and

$$\mathbf{MAP} = \begin{bmatrix} 209.4125 \\ 0.2551 \\ 2.1266 \\ 0.597 \end{bmatrix} \text{ GPa}. \quad (112)$$

The possible stress-strain responses using the 95% credible region for the posterior are presented in Fig. 14.

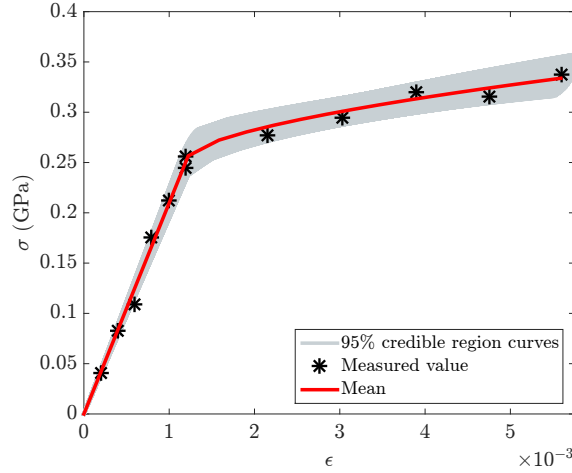


Figure 14: LE-NH: The measurements and the stress-strain curves created using the posterior.

## 5.2. Bayesian inference with noise in stress and strain

All the measurements used in the subsection 5.1 are assumed to be exact in the strain. The aim of current subsection is to show how the previous results change when the strain is also contaminated by noise. To accurately investigate the influence of this, exactly the same measurements are used as in the previous subsection.

### 5.2.1. Linear elastic (LE)

In the first example the same specimen and the same measurements as in subsection 5.1.1 ( $E = 210$  GPa) are considered. The noise distribution obtained from the ‘calibration experiments’ is a normal distribution in the form of Eq. (72) with  $S_\sigma = 0.01$  GPa and  $S_\epsilon = 0.0001$ . For a single measurement pair with  $\sigma^m = 0.1576$  GPa and  $\epsilon^m = 7.25 \times 10^{-4}$ , the posterior distribution can be calculated using Eq. (78). The same prior is selected as in the first example of subsection 5.1.1 ( $\bar{E} = 150$  GPa and  $S_E = 50$  GPa) and the upper limit for the strain is infinity. Running the adaptive MCMC approach for  $10^4$  samples leads to a posterior with  $\mu_{\text{post}} = 202.7767$  GPa,  $S_{\text{post}} = 24.1867$  GPa and MAP = 197.5282 GPa.

Fig. 15 shows the posterior for this case, together with the posterior of subsection 5.1.1 when only the noise in the stress is present. It can clearly be seen that the newly established posterior is wider and it furthermore does not have the form of a (modified) normal distribution, as the posterior when only the noise in the stress is considered.

The stress-strain responses created using the 95% credible region are shown in Fig. 16(a). For comparison, the same responses are shown in Fig. 16(b) when only the stress is polluted by noise. The estimated values for this case are  $\mu_{\text{post}} = 209.1364$  GPa,  $S_{\text{post}} = 9.6642$  GPa and MAP = 207.9963 GPa.

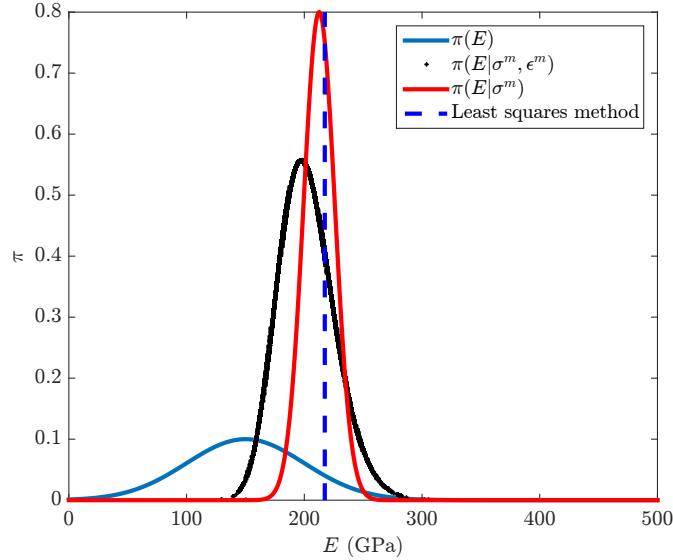
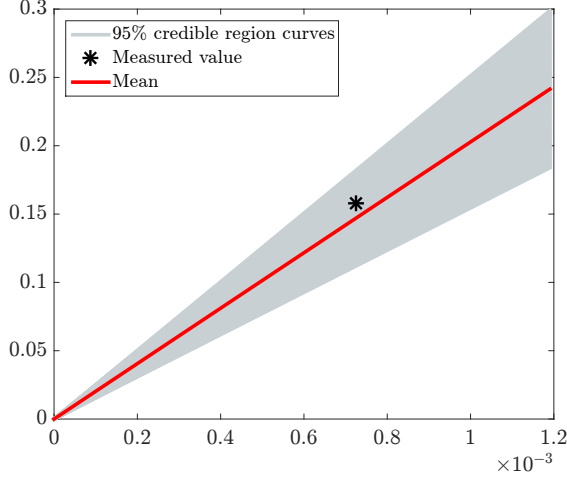
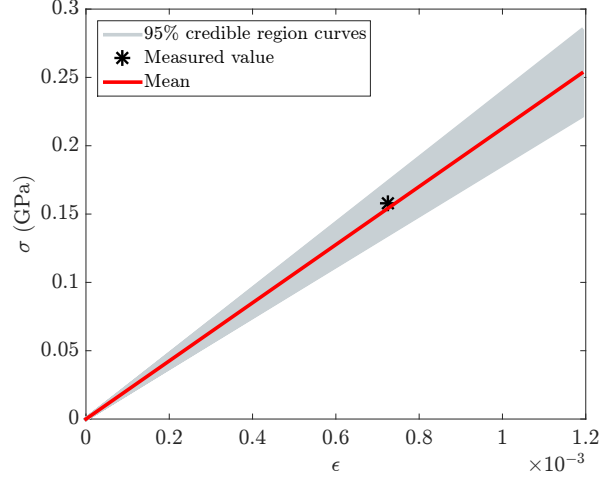


Figure 15: LE: The prior, posterior when both the stress and the strain are corrupted by noise (black dots), the posterior when only the stress is contaminated (red) and the value predicted by the least squares method (blue dashed). The that the newly established posterior is wider and it furthermore does not have the form of a (modified) normal. The distributions are not normalised.

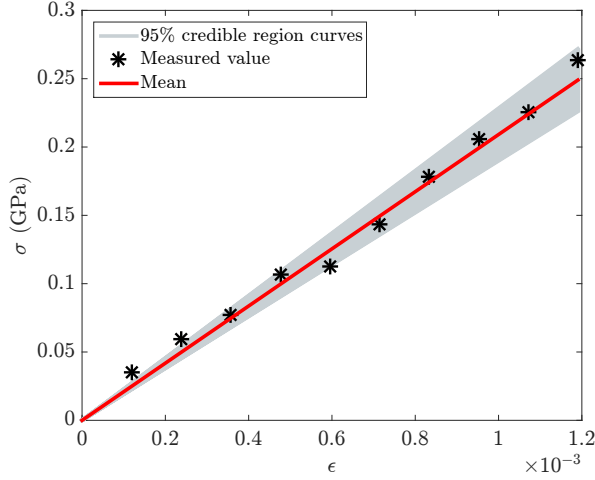


(a) Uncertainty in both the stress and the strain measurements

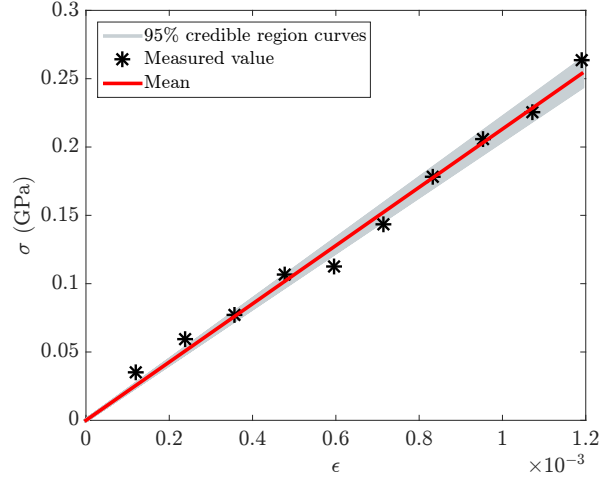


(b) Uncertainty in the stress only

Figure 16: LE: The measurements, and the stress-strain curves created using the posterior for (a) noise in the stress and strain and (b) noise in the stress only. When noise in the stress and strain is considered, the posterior is wider, resulting in a wider 95% credible region.



(a) Uncertainty in both the stress and the strain measurements



(b) Uncertainty in the stress only

Figure 17: LE: The measurements, and the stress-strain curves created using the posterior for ten measurements (a) noise in the stress and the strain and (b) noise in the stress only. When noise in the stress and strain is considered, the posterior is wider, resulting in a wider 95% credible region.

### 5.2.2. Linear elastic-perfectly plastic (LE-PP)

Similar to the example of subsection 5.1.2, in this subsection a specimen is considered with a Young's modulus  $E = 210$  GPa and an initial yield stress  $\sigma_{y0} = 0.25$  GPa. Furthermore, to be able to compare the current results with those of subsection 5.1.2 the same measurements are used here, together with the same noise distribution as in the previous subsection. The prior distribution is furthermore selected as in Eq. (51)

with its properties given in Eq. (99). The resulting posterior is of the form of Eq. (82) with Eq. (81) as the likelihood function. Similar to subsection 5.1.2, the upper limit for the theoretical strain ( $a$  in Eqs. (70) and (81)) is infinity. Employing the adaptive MCMC approach for  $10^4$  samples results in:

$$\boldsymbol{\mu}_{\text{post}} = \begin{bmatrix} 204.0458 \\ 0.2572 \end{bmatrix} \text{ GPa}, \quad \boldsymbol{\Gamma}_{\text{post}} = \begin{bmatrix} 215.3918 & -6.751 \times 10^{-4} \\ -6.751 \times 10^{-4} & 1.4978 \times 10^{-5} \end{bmatrix} \text{ GPa}^2, \quad (113)$$

and

$$\mathbf{MAP} = \begin{bmatrix} 202.5858 \\ 0.2573 \end{bmatrix} \text{ GPa}. \quad (114)$$

In the posterior covariance matrix  $\boldsymbol{\Gamma}_{\text{post}}$  one can see that the additional uncertainty in the strain measurement has a significant effect on  $(\boldsymbol{\Gamma}_{\text{post}})_{11}$ , as the original value was  $5.5373 \text{ GPa}^2$ . Fig. 18 shows the samples generated by the adaptive MCMC approach to approximate the posterior distribution and the associated 95% credible region.

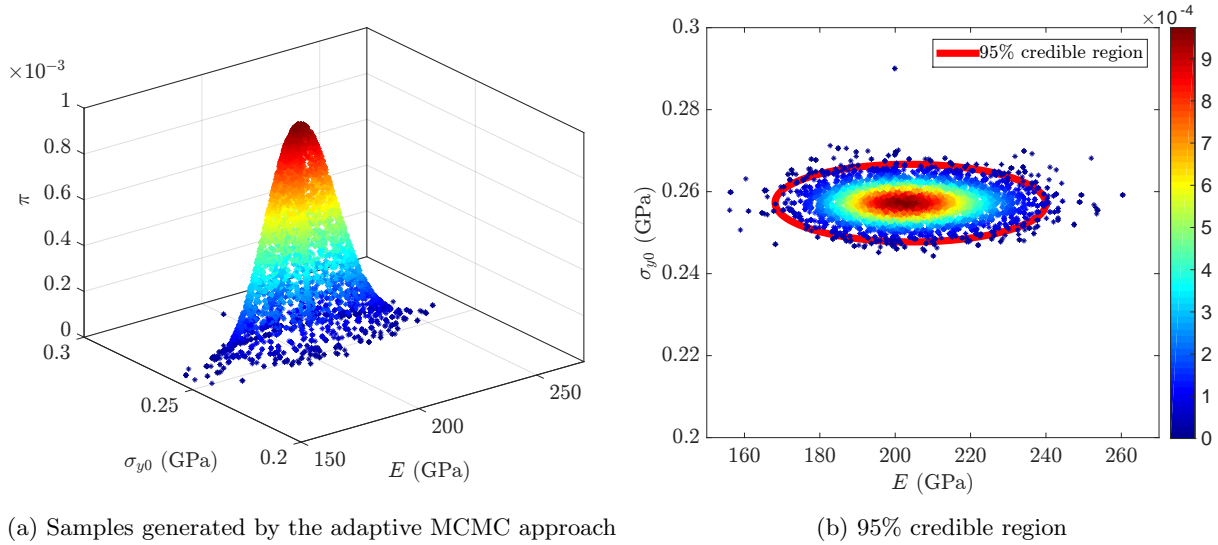


Figure 18: LE-PP: Samples generated by the adaptive MCMC approach to approximate the posterior distribution (a) and the 95% credible region (b).

The stress-strain curves associated with the credible region are shown in Fig. 19(a). The same curves for the case when only the noise in the stress measurements are again presented in Fig. 19(b). Comparing Figs. 19(a) and 19(b), one can see that the uncertainty in the strain has a considerable effect on the elastic response. This is caused by the fact that the plastic part of the response does not depend on the strain. Practically no influence on the yield stress can be observed, because this parameter is independent of the strain.

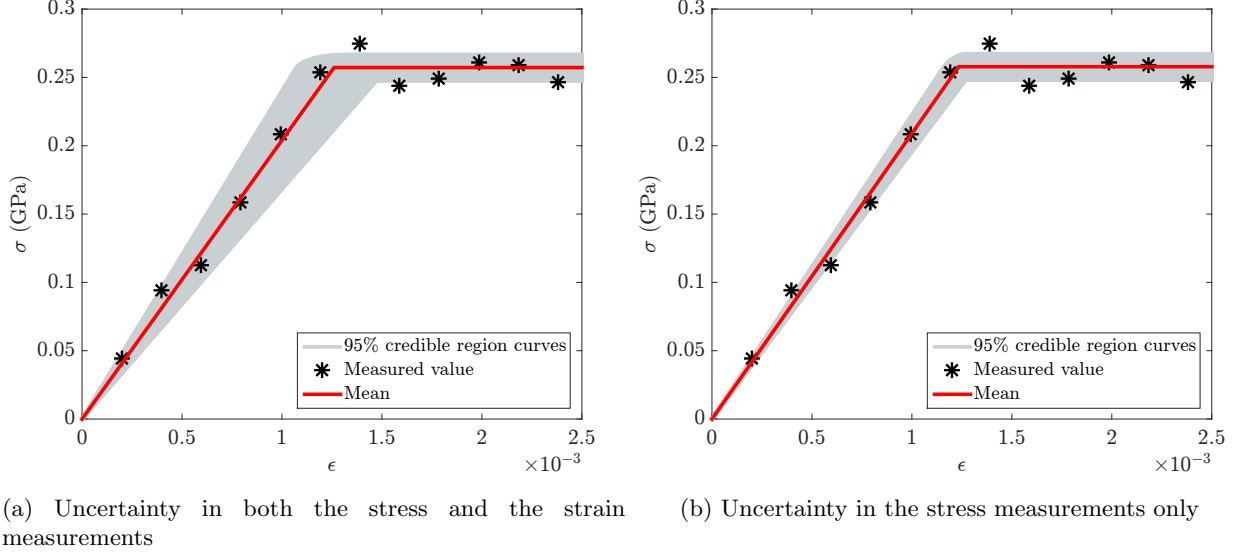


Figure 19: LE-PP: The measurements, and the stress-strain curves created using the posterior for twelve measurements: (a) noise in the stress and strain measurements and (b) noise in the stress measurements only. The uncertainty in the strain has a considerable effect on the elastic response. This is caused by the fact that the plastic part of the response does not depend on the strain.

### 5.2.3. Linear elastic-linear hardening (LE-LH)

In this subsection we will regard the results of the BI formulation for the linear elastic-linear hardening model, when both the stress and the strain measurements are polluted by statistical noise. The same noise model and noise distribution is employed as in the previous subsections. The same measurements as in subsection 5.1.3 are furthermore considered, which are created with  $E = 210$  GPa,  $\sigma_{y0} = 0.25$  GPa and  $H = 50$  GPa. Selecting the prior distribution in the form of Eq. (54) with the mean vector and covariance matrix given by Eq. (107), the resulting posterior is in the form of Eq. (85), where the likelihood function is given by Eq. (83). Employing the adaptive MCMC approach for  $10^4$  sample generations yields:

$$\boldsymbol{\mu}_{\text{post}} = \begin{bmatrix} 204.269 \\ 0.2553 \\ 56.08 \end{bmatrix} \text{ GPa}, \boldsymbol{\Gamma}_{\text{post}} = \begin{bmatrix} 148.2602 & -5.1006 \times 10^{-2} & -14.8463 \\ -5.1006 \times 10^{-2} & 6.0511 \times 10^{-5} & -2.7164 \times 10^{-2} \\ -14.8463 & -2.7164 \times 10^{-2} & 76.7817 \end{bmatrix} \text{ GPa}^2, \quad (115)$$

and

$$\mathbf{MAP} = \begin{bmatrix} 201.8193 \\ 55.0417 \\ 0.256 \end{bmatrix} \text{ GPa}. \quad (116)$$

Similar to in the previous subsections, it is assumed that the theoretical strain ranges from zero to infinity. Comparing the results above with those in Eqs. (108) and (109) shows that the uncertainty in the strain has a larger effect on the Young's modulus and its corresponding components in posterior covariance matrix than on the initial yield stress and the plastic modulus. Fig. 20 shows the samples generated by the adaptive MCMC approach and the associated 95% credible region. The stress strain responses based on the posterior are shown in Fig. 21. The large influence of the noise in the strain measurements on the Young's modulus compared to the influence on the plastic parameters can clearly be distinguished.

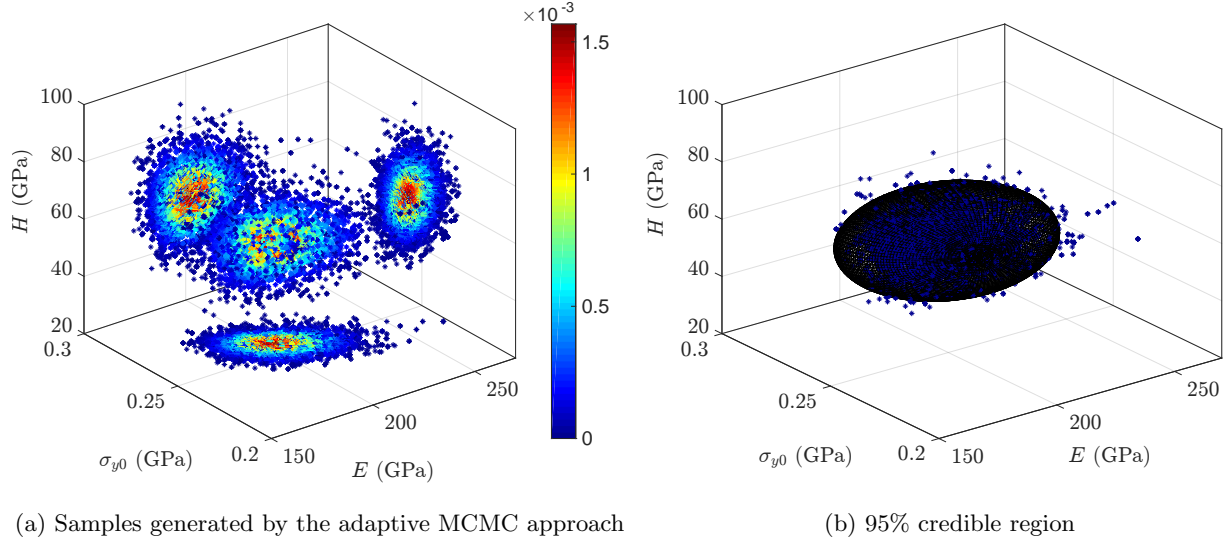


Figure 20: LE-LH: Samples generated by the adaptive MCMC approach to approximate the posterior distribution, its projection on the three planes (a) and the 95% credible region (b).

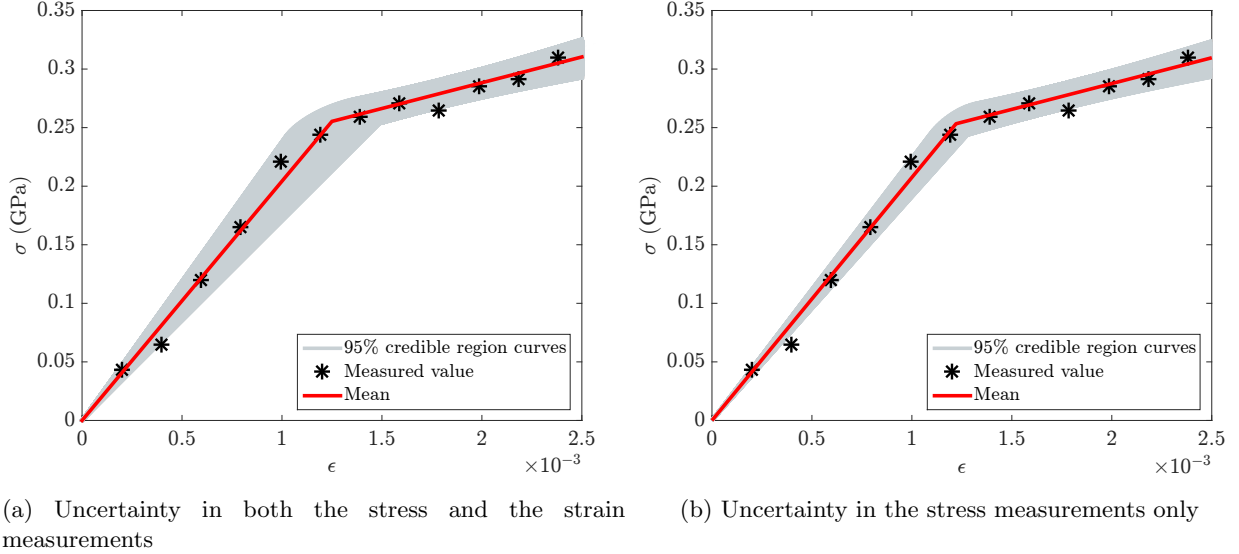


Figure 21: LE-LH: The measurements, and the stress-strain curves created using the posterior for twelve measurements: (a) noise in the stress and strain measurements and (b) noise in the stress measurements only. When noise in the stress and strain is considered, the estimated Young's modulus becomes less certain, but there is hardly any influence on the plastic parameters.

#### 5.2.4. Linear elastic-nonlinear hardening (LE-NH)

The specimen in this subsection is the same as in subsection 5.1.4 and has a Young's modulus  $E = 210$  GPa, an initial yield stress  $\sigma_{y0} = 0.25$  GPa, plastic parameters  $H = 2$  GPa and  $n = 0.57$ . The same measurements as in subsection 5.1.4 are considered as well as the same noise distribution. The prior distribution is in the form of Eq. (64) with its values given in Eq. (110). Consequently, the posterior distribution is in the form of Eq. (97) with the conditional probability  $\pi(\sigma^m | \mathbf{x}, \epsilon^m)$  given by Eq. (91).

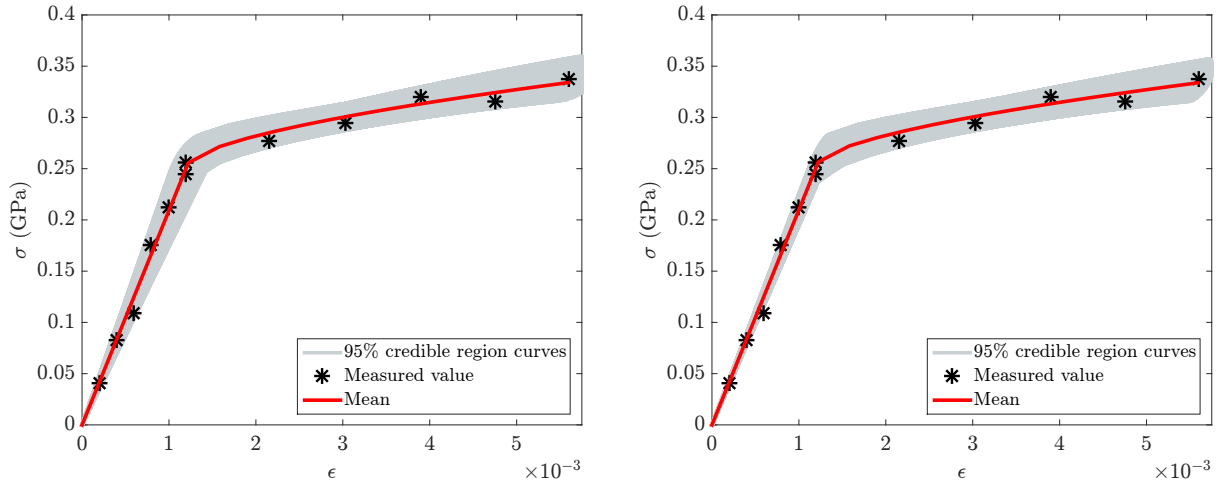
Assuming again that the theoretical strain ranges from zero to infinity and running the adaptive MCMC approach for  $10^4$  samples leads to:

$$\begin{aligned} \boldsymbol{\mu}_{\text{post}} &= \begin{bmatrix} 209.2 \\ 0.2557 \\ 2.1918 \\ 0.6033 \end{bmatrix} \text{ GPa}, \\ \boldsymbol{\Gamma}_{\text{post}} &= \begin{bmatrix} 131.9068 & -2.7875 \times 10^{-2} & 0.4345 & 4.3498 \times 10^{-3} \\ -2.7875 \times 10^{-2} & 8.4839 \times 10^{-5} & -4.9175 \times 10^{-4} & 1.7498 \times 10^{-4} \\ 0.4345 & -4.9175 \times 10^{-4} & 9.925 \times 10^{-2} & 6.1877 \times 10^{-3} \\ 4.3498 \times 10^{-3} & 1.7498 \times 10^{-4} & 6.1873 \times 10^{-3} & 1.1031 \times 10^{-3} \end{bmatrix} \text{ GPa}^2, \end{aligned} \quad (117)$$

and

$$\mathbf{MAP} = \begin{bmatrix} 208.6431 \\ 0.2555 \\ 2.2619 \\ 0.6055 \end{bmatrix} \text{ GPa}. \quad (118)$$

The predicted stress-strain curves using the 95% credible regions are shown in Fig. 22 for both the single uncertainty and the double uncertainty cases. As can be seen, the uncertainty in the strain largely influences the Young's modulus because the multiplied gain to the strain ( $E$ ) in the elastic part is much larger than the gain in plastic part.



(a) Uncertainty in both the stress and the strain measurements

(b) Uncertainty in the stress measurements only

Figure 22: LE-NH: The measurements, and the stress-strain curves created using the posterior for twelve measurements: (a) noise in the stress and strain measurements and (b) noise in the stress measurements only. The uncertainty in the strain largely influences the Young's modulus because the multiplied gain to the strain ( $E$ ) in the elastic part is much larger than the gain in plastic part.

## 6. Conclusion

In this contribution, we have proposed a number of BI formulations to identify elastoplastic material parameters of a single spring based on uniaxial tensile results. The main goals of the paper are:

- (1) to explain and propose BI formulations for the identification of elasto-plastic material parameters, when only the stress measurements are contaminated by statistical noise,
- (2) to propose BI formulations for the identification of elasto-plastic material parameters, when the stress measurements as well as the strain measurements are contaminated by statistical noise,
- (3) expose possible misconceptions of BI.

In order to apply or develop a Bayesian approach, a noise model and noise distribution need to be formulated, based on calibration results. Our calibration results were artificially created, but this has enabled us to clearly investigate the abilities of the BI formulations and to compare the results with those of the least squares method.

We have only considered an additive noise model and a normal noise distribution. Although this is somewhat limited, we have considered this noise model and distribution because we believe they are most often required and were most often used in the existing literature. The main focus of this study was furthermore on the application of Bayesian updating for several elastoplastic models. The BI formulations ranged from a simple linear elastic model to more complicated ones, such as the linear elastic-nonlinear hardening model. We have only analysed the posterior distribution of the linear elastic model with noise in the stress measurements analytically. All other posteriors were required to be numerically approximated using an adaptive Markov chain Monte Carlo approach, which was discussed in subsection 2.3.

The examples given in the section 5 indicate a number of issues that may be not trivial to grasp for researchers new to BI:

- (1) The results of BI cannot directly be compared to those of the least squares method. BI assumes that other measurements could have been made and hence, the actual measurements are only (a limited number of) realisations of statistical distributions. BI aims to take this awareness into account (via the prior distribution).
- (2) If one however wants to compare the results of both approaches, it is shown in Fig. 3(a) that the selected prior distribution has a significant effect on the results. Fig. 3(a) also shows that the influence of the prior decreases significantly if the number of measurements increases.
- (3) The standard deviations and correlations of the material parameters established using the ‘standard’ BI formulations presented in this contribution, do *not* reflect the heterogeneity of the material parameters. In other words, they are *not* representative for the standard deviations and correlations of the material parameter distributions. Hence, they are only a measure for the uncertainty of the mean values and MAP points. If one wants to find the actual distributions of the material parameters, the ‘standard’ BI formulations presented here need to be extended. This is the focus of our future work.
- (4) Comparing of the results when only the stress measurements are polluted by statistical noise to those when also the strain measurements are polluted by statistical noise, has shown that the uncertainty of the Young’s modulus is substantially influenced by the noise in the strain measurements. The influence on the uncertainty of the plastic parameters is quite limited however. It may therefore be worthwhile to consider noise in the strains (next to noise in the stresses) when one is interested in elastic parameters. If one is mostly interested in the plastic parameters however, it seems questionable if the substantially more complex BI formulations for double error sources are worth the extra efforts.

## References

## References

- [1] C. Gogu, R. Haftka, R. L. Riche, J. Molimard, A. Vautrin, Introduction to the bayesian approach applied to elastic constants identification, AIAA journal 48 (5) (2010) 893–903.



- [2] D. Higdon, H. Lee, Z. Bi, A bayesian approach to characterizing uncertainty in inverse problems using coarse and fine scale information, *IEEE Transactions on Signal Processing* 50 (2002) 388–399.
- [3] J. Wang, N. Zabaras, A bayesian inference approach to the inverse heat conduction problem, *International Journal of Heat and Mass Transfer* 47 (1718) (2004) 3927 – 3941. doi:<http://dx.doi.org/10.1016/j.ijheatmasstransfer.2004.02.028>.
- [4] P. Risholm, F. Janoos, I. Norton, A. J. Golby, W. M. Wells, Bayesian characterization of uncertainty in intra-subject non-rigid registration, *Medical image analysis* 17 (5) (2013) 538–555. doi:<http://dx.doi.org/10.1016/j.media.2013.03.002>.
- [5] S. Lan, T. Bui-Thanh, M. Christie, M. Girolami, Emulation of higher-order tensors in manifold monte carlo methods for bayesian inverse problems, *Journal of Computational Physics* 308 (2016) 81 – 101. doi:<http://dx.doi.org/10.1016/j.jcp.2015.12.032>.
- [6] J. Beck, L. Katafygiotis, Updating models and their uncertainties. i: Bayesian statistical framework, *Journal of Engineering Mechanics* 124 (4) (1998) 455–461. doi:[10.1061/\(ASCE\)0733-9399\(1998\)124:4\(455\)](https://doi.org/10.1061/(ASCE)0733-9399(1998)124:4(455)).
- [7] C. K. Oh, J. L. Beck, M. Yamada, Bayesian learning using automatic relevance determination prior with an application to earthquake early warning, *Journal of Engineering Mechanics* 134 (12) (2008) 1013–1020. doi:[10.1061/\(ASCE\)0733-9399\(2008\)134:12\(1013\)](https://doi.org/10.1061/(ASCE)0733-9399(2008)134:12(1013)).
- [8] J. Kaipio, E. Somersalo, *Statistical and computational inverse problems*, Vol. 160, Springer Science & Business Media, 2006.
- [9] J. Isenberg, Progressing from Least Squares to Bayesian Estimation, *Proceedings of the 1979 ACME Design Engineering Technical Conference*, New York (1979) 1–11.
- [10] K. Alvin, Finite element model update via bayesian estimation and minimization of dynamic residuals, *AIAA journal* 35 (5) (1997) 879–886. doi:[10.2514/2.7462](https://doi.org/10.2514/2.7462).
- [11] T. Marwala, S. Sibusiso, Finite element model updating using bayesian framework and modal properties, *Journal of Aircraft* 42 (1) (2005) 275–278. doi:[10.2514/1.11841](https://doi.org/10.2514/1.11841).
- [12] T. Lai, K. Ip, Parameter estimation of orthotropic plates by bayesian sensitivity analysis, *Composite Structures* 34 (1) (1996) 29 – 42. doi:[http://dx.doi.org/10.1016/0263-8223\(95\)00128-X](http://dx.doi.org/10.1016/0263-8223(95)00128-X).
- [13] F. Daghia, S. de Miranda, F. Ubertini, E. Viola, Estimation of elastic constants of thick laminated plates within a bayesian framework, *Composite Structures* 80 (3) (2007) 461 – 473. doi:<http://dx.doi.org/10.1016/j.compstruct.2006.06.030>.
- [14] P.-S. Koutsourelakis, A novel bayesian strategy for the identification of spatially varying material properties and model validation: an application to static elastography, *International Journal for Numerical Methods in Engineering* 91 (3) (2012) 249–268. doi:[10.1002/nme.4261](https://doi.org/10.1002/nme.4261).
- [15] C. Gogu, W. Yin, R. Haftka, P. Ifju, J. Molimard, R. Le Riche, A. Vautrin, Bayesian identification of elastic constants in multi-directional laminate from moiré interferometry displacement fields, *Experimental Mechanics* 53 (4) (2013) 635–648. doi:[10.1007/s11340-012-9671-8](https://doi.org/10.1007/s11340-012-9671-8).
- [16] M. Muto, J. L. Beck, Bayesian updating and model class selection for hysteretic structural models using stochastic simulation, *Journal of Vibration and Control* 14 (1-2) (2008) 7–34. doi:[10.1177/1077546307079400](https://doi.org/10.1177/1077546307079400).
- [17] P. Liu, S.-K. Au, Bayesian parameter identification of hysteretic behavior of composite walls, *Probabilistic Engineering Mechanics* 34 (2013) 101 – 109. doi:<http://dx.doi.org/10.1016/j.probengmech.2013.08.005>.

- [18] D. D. Fitzenz, A. Jalobeanu, S. H. Hickman, Integrating laboratory creep compaction data with numerical fault models: A bayesian framework, *Journal of Geophysical Research: Solid Earth* 112 (B8) (2007) n/a–n/a, b08410. doi:[10.1029/2006JB004792](https://doi.org/10.1029/2006JB004792).
- [19] T. Most, Identification of the parameters of complex constitutive models: Least squares minimization vs. bayesian updating, *Reliability and Optimization of Structural Systems* (2010) 119.
- [20] B. V. Rosic, A. Kucerova, J. Sykora, O. Pajonk, A. Litvinenko, H. G. Matthies, Parameter identification in a probabilistic setting, *Engineering Structures* 50 (2013) 179 – 196, engineering Structures: Modelling and Computations (special issue IASS-IACM 2012). doi:<http://dx.doi.org/10.1016/j.engstruct.2012.12.029>.
- [21] W. Hernandez, F. Borges, D. Castello, N. Roitman, C. Magluta, Bayesian inference applied on model calibration of fractional derivative viscoelastic model, in: *DINAME 2015 - Proceedings of the XVII International Symposium on Dynamic Problems of Mechanics*, 2015.
- [22] J. Nichols, W. Link, K. Murphy, C. Olson, A bayesian approach to identifying structural nonlinearity using free-decay response: Application to damage detection in composites, *Journal of Sound and Vibration* 329 (15) (2010) 2995 – 3007. doi:<http://dx.doi.org/10.1016/j.jsv.2010.02.004>.
- [23] S. Abhinav, C. Manohar, Bayesian parameter identification in dynamic state space models using modified measurement equations, *International Journal of Non-Linear Mechanics* 71 (2015) 89 – 103. doi:<http://dx.doi.org/10.1016/j.ijnonlinmec.2015.02.003>.
- [24] S. Madireddy, B. Sista, K. Vemaganti, A bayesian approach to selecting hyperelastic constitutive models of soft tissue, *Computer Methods in Applied Mechanics and Engineering* 291 (2015) 102 – 122. doi:<http://dx.doi.org/10.1016/j.cma.2015.03.012>.
- [25] J. T. Oden, E. E. Prudencio, A. Hawkins-Daarud, Selection and assesment of phenomenological models of tumor growth, *Mathematical Models and Methods in Applied Sciences* 23 (07) (2013) 1309–1338. arXiv:<http://www.worldscientific.com/doi/pdf/10.1142/S0218202513500103>, doi:[10.1142/S0218202513500103](https://doi.org/10.1142/S0218202513500103).
- [26] J. Chiacho, M. Chiacho, A. Saxena, S. Sankararaman, G. Rus, K. Goebel, Bayesian model selection and parameter estimation for fatigue damage progression models in composites, *International Journal of Fatigue* 70 (2015) 361 – 373. doi:<http://dx.doi.org/10.1016/j.ijfatigue.2014.08.003>.
- [27] I. Babuska, Z. Sawlan, M. Scavino, B. Szabo, R. Tempone, Bayesian inference and model comparison for metallic fatigue data, *Computer Methods in Applied Mechanics and Engineering* 304 (2016) 171 – 196. doi:<http://dx.doi.org/10.1016/j.cma.2016.02.013>.
- [28] S. Sarkar, D. Kosson, S. Mahadevan, J. Meeussen, H. van der Sloot, J. Arnold, K. Brown, Bayesian calibration of thermodynamic parameters for geochemical speciation modeling of cementitious materials, *Cement and Concrete Research* 42 (7) (2012) 889 – 902. doi:<http://dx.doi.org/10.1016/j.cemconres.2012.02.004>.
- [29] S. L. Cotter, M. Dashti, J. C. Robinson, A. M. Stuart, Bayesian inverse problems for functions and applications to fluid mechanics, *Inverse Problems* 25 (11) (2009) 115008. doi:<http://dx.doi.org/10.1088/0266-5611/25/11/115008>.
- [30] S. Gull, Bayesian data analysis: Straight-line fitting, in: J. Skilling (Ed.), *Maximum Entropy and Bayesian Methods*, Vol. 36 of *Fundamental Theories of Physics*, Springer Netherlands, 1989, pp. 511–518. doi:[10.1007/978-94-015-7860-8\\_55](https://doi.org/10.1007/978-94-015-7860-8_55).
- [31] D. A. S. Petros Dellaportas, Bayesian analysis of errors-in-variables regression models, *Biometrics* 51 (3) (1995) 1085–1095. doi:[10.2307/2533007](https://doi.org/10.2307/2533007).

- [32] L. W. Raymond J. Carroll, Kathryn Roeder, Flexible parametric measurement error models, *Biometrics* 55 (1) (1999) 44–54. doi:10.2307/2533894.
- [33] R. Scheines, H. Hoijtink, A. Boomsma, Bayesian estimation and testing of structural equation models, *Psychometrika* 64 (1) (1999) 37–52. doi:10.1007/BF02294318.
- [34] B. C. Kelly, Some aspects of measurement error in linear regression of astronomical data, *The Astrophysical Journal* 665 (2) (2007) 1489. doi:http://dx.doi.org/10.1086/519947.
- [35] D. W. Hogg, J. Bovy, D. Lang, Data analysis recipes: Fitting a model to data, *ArXiv e-prints* arXiv:1008.4686.
- [36] A. van der Vaart, *Asymptotic Statistics*, Cambridge University Press, 1998.
- [37] T. J. Ulrych, M. D. Sacchi, A. Woodbury, A bayes tour of inversion: A tutorial, *GEOPHYSICS* 66 (1) (2001) 55–69. arXiv:http://dx.doi.org/10.1190/1.1444923, doi:10.1190/1.1444923.
- [38] J. Simo, T. Hughes, *Computational Inelasticity*, Springer New York, 2000.
- [39] J. L. Beck, S.-K. Au, Bayesian updating of structural models and reliability using markov chain monte carlo simulation, *Journal of Engineering Mechanics* 128 (4) (2002) 380–391. doi:10.1061/(ASCE)0733-9399(2002)128:4(380).
- [40] Y. M. Marzouk, H. N. Najm, L. A. Rahn, Stochastic spectral methods for efficient bayesian solution of inverse problems, *Journal of Computational Physics* 224 (2) (2007) 560 – 586. doi:http://dx.doi.org/10.1016/j.jcp.2006.10.010.
- [41] J. Kristensen, N. J. Zabaras, Bayesian uncertainty quantification in the evaluation of alloy properties with the cluster expansion method, *Computer Physics Communications* 185 (11) (2014) 2885 – 2892. doi:http://dx.doi.org/10.1016/j.cpc.2014.07.013.
- [42] C. Andrieu, N. De Freitas, A. Doucet, M. I. Jordan, An introduction to mcmc for machine learning, *Machine learning* 50 (1-2) (2003) 5–43. doi:10.1023/A:1020281327116.
- [43] S. Brooks, A. Gelman, G. Jones, X.-L. Meng, *Handbook of Markov chain Monte Carlo*, CRC press, 2011.
- [44] A. Gelman, G. O. Roberts, W. R. Gilks, Efficient Metropolis jumping rules, in: *Bayesian statistics*, 5 (Alicante, 1994), Oxford Sci. Publ., Oxford Univ. Press, New York, 1996, pp. 599–607.
- [45] H. Haario, E. Saksman, J. Tamminen, Adaptive proposal distribution for random walk metropolis algorithm, *Computational Statistics* 14 (3) (1999) 375–396.
- [46] A. Gelman, J. Carlin, H. Stern, D. Rubin, *Bayesian data analysis*, Chapman & Hall/CRC Texts in Statistical Science, Chapman & Hall/CRC, 2003.
- [47] S. Hassani, *Mathematical methods: for students of physics and related fields*, Springer New York, 2008.
- [48] S. Prince, *Computer vision: models learning and inference*, Cambridge University Press, 2012.